




















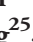






Acclimation and adaptation components of the temperature dependence of plant photosynthesis at the global scale

Dushan P. Kumarathunge^{1,2} , Belinda E. Medlyn¹ , John E. Drake³ , Mark G. Tjoelker¹ , Michael J. Aspinwall⁴ , Michael Battaglia⁵, Francisco J. Cano¹ , Kelsey R. Carter⁶ , Molly A. Cavaleri⁶ , Lucas A. Cernusak⁷ , Jeffrey Q. Chambers⁸ , Kristine Y. Crous¹ , Martin G. De Kauwe⁹ , Dylan N. Dillaway¹⁰, Erwin Dreyer¹¹ , David S. Ellsworth¹ , Oula Ghannoum¹ , Qingmin Han¹², Kouki Hikosaka¹³, Anna M. Jensen¹⁴ , Jeff W. G. Kelly¹⁵, Eric L. Kruger¹⁶, Lina M. Mercado^{17,18} , Yusuke Onoda¹⁹ , Peter B. Reich^{1,20} , Alistair Rogers²¹ , Martijn Slot²² , Nicholas G. Smith²³ , Lasse Tarvainen^{24,25} , David T. Tissue¹ , Henrique F. Togashi²⁶, Edgar S. Tribuzy²⁷, Johan Uddling²⁵, Angelica Varhammar¹, Göran Wallin²⁵ , Jeffrey M. Warren²⁸ and Danielle A. Way^{29,30} 

¹Hawkesbury Institute for the Environment, Western Sydney University, Locked Bag 1797, Penrith, NSW 2751, Australia; ²Plant Physiology Division, Coconut Research Institute of Sri Lanka, Lunuwila 61150, Sri Lanka; ³Forest and Natural Resources Management, College of Environmental Science and Forestry, State University of New York, 1 Forestry Drive, Syracuse, NY 13210, USA; ⁴Department of Biology, University of North Florida, 1 UNF Drive, Jacksonville, FL 32224, USA; ⁵CSIRO Agriculture and Food, Private Bag 12, Hobart, Tasmania 7001, Australia; ⁶School of Forest Resources & Environmental Science, Michigan Technological University, 1400 Townsend Dr., Houghton, MI 49931, USA; ⁷College of Science and Engineering, James Cook University, Cairns, QLD 4878, Australia; ⁸Department of Geography, University of California Berkeley, 507 McCone Hall #4740, Berkeley, CA 94720, USA; ⁹ARC Centre of Excellence for Climate Extremes, University of New South Wales, Sydney, NSW 2052, Australia; ¹⁰Thomashow Learning Laboratories, Unity College, 90 Quaker Hill Road, Unity, ME 04988, USA; ¹¹Université de Lorraine, Inra, Silva, F54000 Nancy, France; ¹²Department of Plant Ecology, Forestry and Forest Products Research Institute (FFPRI), 1 Matsunosato, Tsukuba, Ibaraki 305-8687, Japan; ¹³Graduate School of Life Sciences, Tohoku University, Aoba Sendai 980-8578, Japan; ¹⁴Department of Forestry and Wood Technology, Linnaeus University, Växjö, Sweden; ¹⁵Center for Sustainable Forestry at Pack Forest, University of Washington, 9010 453rd Street E, Eatonville, WA 98328, USA; ¹⁶Department of Atmospheric and Oceanic Sciences, University of Wisconsin-Madison, Madison, WI 53706, USA; ¹⁷College of Life and Environmental Sciences, University of Exeter, Exeter, EX4 4PS, UK; ¹⁸Centre for Ecology and Hydrology, Crowmarsh-Gifford, Wallingford, OX10 8BB, UK; ¹⁹Graduate School of Agriculture, Kyoto University, Kyoto 606-8502, Japan; ²⁰Department of Forest Resources, University of Minnesota, St Paul, MN 55108, USA; ²¹Environmental and Climate Sciences Department, Brookhaven National Laboratory, Upton, NY 11973-5000, USA; ²²Smithsonian Tropical Research Institute, Apartado 0843-03092, Balboa, Ancón, Panama; ²³Department of Biological Sciences, Texas Tech University, Lubbock, TX, USA; ²⁴Department of Forest Ecology and Management, Swedish University of Agricultural Sciences (SLU), SE-901 83, Umeå, Sweden; ²⁵Department of Biological and Environmental Sciences, University of Gothenburg, PO Box 461, Gothenburg SE-405 30, Sweden; ²⁶Department of Biological Sciences, Macquarie University, North Ryde, NSW 2109, Australia; ²⁷Instituto de Biodiversidade e Florestas, Universidade Federal do Oeste do Pará (UFOPA), CEP 68035-110, Santarém, PA, Brazil; ²⁸Climate Change Science Institute and Environmental Sciences Division, Oak Ridge National Laboratory, Oak Ridge, TN 37831, USA; ²⁹Department of Biology, The University of Western Ontario, London, ON Canada, N6A 5B6; ³⁰Nicholas School of the Environment, Duke University, Box 90328, Durham, NC 27708, USA

Summary

Author for correspondence:
Dushan P. Kumarathunge
Tel: +614 78807875
Email:
d.kumarathunge@westernsydney.edu.au

Received: 27 July 2018
Accepted: 7 December 2018

New Phytologist (2019) 222: 768–784
doi: 10.1111/nph.15668

Key words: AC_i curves, climate of origin, global vegetation models (GVMs), growth temperature, J_{\max} , maximum carboxylation capacity, maximum electron transport rate, V_{\max} .

- The temperature response of photosynthesis is one of the key factors determining predicted responses to warming in global vegetation models (GVMs). The response may vary geographically, owing to genetic adaptation to climate, and temporally, as a result of acclimation to changes in ambient temperature. Our goal was to develop a robust quantitative global model representing acclimation and adaptation of photosynthetic temperature responses.
- We quantified and modelled key mechanisms responsible for photosynthetic temperature acclimation and adaptation using a global dataset of photosynthetic CO₂ response curves, including data from 141 C₃ species from tropical rainforest to Arctic tundra. We separated temperature acclimation and adaptation processes by considering seasonal and common-garden datasets, respectively.
- The observed global variation in the temperature optimum of photosynthesis was primarily explained by biochemical limitations to photosynthesis, rather than stomatal conductance or respiration. **We found acclimation to growth temperature to be a stronger driver of this variation than adaptation to temperature at climate of origin.**
- We developed a summary model to represent photosynthetic temperature responses and showed that it predicted the observed global variation in optimal temperatures with high accuracy. This novel algorithm should enable improved prediction of the function of global ecosystems in a warming climate.

Introduction

The capacity of species to cope with increasing growth temperature is one of the key determinants in range shifts and local extinction of species, because their distribution and range limits closely follow temperature isolines (Battisti *et al.*, 2005). Evidence suggests that many species are adapted to their thermal environment of origin (Berry & Björkman, 1980) but also exhibit the capacity to adjust to temporal variations in the temperature of their environment (Rehfeldt *et al.*, 2001; Valladares *et al.*, 2014). However, the mechanisms that determine these responses are not well understood, making it challenging to predict the fate of plants in a changing climate.

Global vegetation models (GVMs) are one of the principal tools used to predict future terrestrial vegetation carbon (C) balance (Rogers *et al.*, 2017a; Mercado *et al.*, 2018). The temperature response of leaf-scale net photosynthesis (referred to as A_n - T response hereafter) is one of the key processes in these models. The effect of warming on modelled photosynthesis depends on the A_n - T response function used in the model and, in particular, the optimum temperature of photosynthesis (T_{optA} ; Booth *et al.*, 2012). Decades of empirical studies have shown that the A_n - T responses of plants vary geographically, suggesting genetic adaptation of species to their climate of origin (Fryer & Ledig, 1972; Slatyer, 1977, 1978; Berry & Björkman, 1980; Gunderson *et al.*, 2009). Considerable evidence also shows that plants have the capacity to adjust the A_n - T response following temporal changes in ambient temperature, a response known as thermal acclimation (Way & Sage, 2008; Hall *et al.*, 2013; Way & Yamori, 2014; Yamaguchi *et al.*, 2016; Way *et al.*, 2017). In a recent review, Yamori *et al.* (2014) reported inherent differences in the A_n - T response and its acclimation capacity among photosynthetic pathways (C_3 , C_4 and CAM) and functional types (annual vs perennial, deciduous vs evergreen) that often differ in their climatic distributions. However, the current representations of A_n - T response in GVMs do not capture this empirical knowledge well (Smith & Dukes, 2013; Lombardozzi *et al.*, 2015; Smith *et al.*, 2016; Mercado *et al.*, 2018). Most GVMs use either a single A_n - T response function for all species or represent broad geographical variation in the A_n - T response by using plant functional type (PFT)-specific functions without considering thermal acclimation. Robust representation of adaptation and acclimation of A_n - T response in GVMs is challenging, as we lack a quantitative assessment of acclimation and adaptation of photosynthetic temperature responses on a global scale (Stinziano *et al.*, 2017).

Many GVMs incorporate the biochemical model of C_3 photosynthesis (referred to as FvCB hereafter; Farquhar *et al.*, 1980; Rogers *et al.*, 2017a). Therefore, it is both tractable and valuable to encapsulate the mechanisms of photosynthetic temperature adaptation and acclimation in terms of parameters of the Farquhar model (Hikosaka *et al.*, 1999; Dreyer *et al.*, 2001; Medlyn *et al.*, 2002b; Dillaway & Kruger, 2010). The model has two key parameters, for which the temperature response is particularly important: the maximum rate of ribulose-1,5-bisphosphate carboxylase-oxygenase (Rubisco) activity (V_{cmax}) and the

potential electron transport rate (J_{max}) (Farquhar *et al.*, 1980). GVMs use two basic functional forms to characterize the instantaneous temperature response of the key FvCB model parameters, namely the standard and peaked Arrhenius functions (Medlyn *et al.*, 2002a). Most empirical studies of the instantaneous temperature response of V_{cmax} and J_{max} have used the peaked Arrhenius model, which has four key parameters: the basal rate of either V_{cmax} or J_{max} at a standard temperature of 25°C (V_{cmax25} or J_{max25}), the activation energy (E_a), the deactivation energy (H_d) and the entropy term (ΔS). The peaked Arrhenius model can also be used to calculate the optimum temperatures of V_{cmax} (T_{optV}) and J_{max} (T_{optJ}). These parameters have now been documented for a wide range of species from different biomes and PFTs (Onoda *et al.*, 2005; Rogers *et al.*, 2017b; Slot & Winter, 2017). Evidence suggests that the Arrhenius model parameters vary significantly across plant taxa but also that these parameters have the capacity to acclimate to the growth temperature (Crous *et al.*, 2013, 2018).

Several meta-analytic studies have attempted to characterize species variation in the model parameters. Medlyn *et al.* (2002a) compared the temperature response of key FvCB model parameters across different species but reported a poor relationship overall between the optimum temperature for photosynthesis and the temperature of the growing environment. They reported lower T_{optV} and T_{optJ} for plants grown in boreal vs temperate climates, but it was unclear whether this difference was a result of inherent genetic differences among the boreal and temperate species, or of acclimation to prevailing growth temperature. In an analysis of 23 species, Hikosaka *et al.* (2006) identified two important mechanisms of photosynthetic temperature acclimation, namely E_a of V_{cmax} (E_{aV}) and J_{max} (E_{aJ}) and the ratio $J_{max} : V_{cmax}$ (JV_r). The most comprehensive synthesis to date of the biochemically based plant photosynthetic temperature response is that of Kattge & Knorr (2007), who compared the instantaneous temperature response of V_{cmax} and J_{max} across 36 species. This study found a lack of thermal acclimation of E_{aV} and E_{aJ} , but reported significant acclimation relationships for JV_r and ΔS of V_{cmax} (ΔS_V) and J_{max} (ΔS_J). Importantly, Kattge & Knorr (2007) synthesized these relationships into a simple and generalizable form that enabled direct implementation into GVMs, thus providing a means to quantify the effect of thermal acclimation of photosynthesis on terrestrial C cycle predictions (Chen & Zhuang, 2013; Lombardozzi *et al.*, 2015; Smith *et al.*, 2016) as well as on biophysical consequences in future climates (Smith *et al.*, 2017).

Despite the success of the Kattge & Knorr (2007) algorithms, the functions have several limitations. Firstly, the parameterization process did not consider potential interspecific differences in photosynthetic temperature response; all changes were attributed to differences in growth temperature. Hence, the response incorporates elements of both temperature adaptation and acclimation without resolving the extent of the contribution of the two processes. Given that acclimation can occur over days and that adaptation takes many generations, the importance of resolving the relative contribution of the two processes is critical. Recently, Mercado *et al.* (2018) showed that assuming the relationships

represent both adaptation and acclimation, or adaptation only, leads to significantly different conclusions about the trajectory of future terrestrial C storage under warming. Their results further highlight the importance of separating photosynthetic thermal adaptation and acclimation when simulating current and future C storage. However, to date, few studies have separated species differences in temperature adaptation from temperature acclimation processes (Lin *et al.*, 2013).

Second, the data used to derive the Kattge & Knorr (2007) functions came mainly from northern temperate and boreal trees and lacked globally important PFTs such as tropical forests and Arctic tundra. As a result, the growth temperature range varied only from 11 to 29°C (Kattge & Knorr, 2007), which is substantially narrower than growth temperatures simulated in GVMs. Therefore, the analysis of Kattge & Knorr (2007) could be improved with a broader global dataset directly addressing the relative roles of temperature acclimation and adaptation.

Third, the ability of the acclimation functions to capture the observed differences in temperature optima of light-saturated net photosynthesis (T_{optA}) has not been directly tested. It is not clear whether making adjustments to T_{optV} and T_{optJ} improves the ability of models to capture changes in T_{optA} ; some studies have reported similar T_{optA} values even with significantly different T_{optJ} among species (Vårhammar *et al.*, 2015). Moreover, the photosynthetic temperature response is controlled not only by the photosynthetic biochemistry, but also by stomatal and respiratory processes. Sensitivity analysis suggests that all three component processes are equally important in determining the T_{optA} at leaf scale (Lin *et al.*, 2012) as well as at canopy scale (Tan *et al.*, 2017) but none of the previous review studies addressed how the latter two components affected T_{optA} .

Given the need for robust representation of photosynthetic temperature acclimation and adaptation in GVMs, and its importance in predicting future global C budget (Lombardozzi *et al.*, 2015; Smith *et al.*, 2016; Mercado *et al.*, 2018) and climate (Smith *et al.*, 2017), we quantified and modelled the mechanisms that underlie the observed differences in T_{optA} among species and growth temperatures. We hypothesized that T_{optA} would be strongly driven by adaptation to the climate of origin, whereas temperature acclimation would further modify the temperature optimum in response to seasonal changes in temperature of the growth environment. To test these hypotheses, we compiled a global database of photosynthetic CO₂ response curves measured at multiple leaf temperatures to simultaneously resolve the temperature optima of A_{net} , V_{cmax} and J_{max} . The data comprised a total of 141 species from tropical rainforests to Arctic tundra. Included in this database were datasets from common-garden studies, which were used to quantify effects of adaptation alone on T_{optA} , and comprising time course studies that measured plants under contrasting prevailing ambient temperatures, which are used to quantify effects of temperature acclimation alone. We combined the identified effects of climate adaptation and temperature acclimation to derive a general global model of temperature responses, which is then tested against a third, independent, biogeographic dataset measured on mature plants growing in their native environments across the globe.

Materials and Methods

Data sources

We compiled a global database of datasets consisting of leaf photosynthetic CO₂ response measurements (referred to as ACi curves hereafter) measured at multiple leaf temperatures and saturating irradiance intensities. The database covers 141 species from 38 experiments conducted around the world (Supporting Information Fig. S1; Table S1). Site latitude ranged from 42°48'S to 71°16'N, and mean annual growing season temperature (long-term average temperature of months where mean monthly temperature is > 0°C) ranged from 3 to 30°C.

The method of data collection was consistent across all datasets. In most datasets, measurements were started at ambient CO₂ concentrations (360–400 ppm; depending on the year of data collection) and changed stepwise through a series of subambient (40–400 ppm) to superambient saturating CO₂ concentrations (400–2000 ppm). The same measurement protocol was repeated on the same leaf at different leaf temperatures. Measurements were made at saturating irradiance (Table S1) using a portable photosynthesis system with standard leaf chambers, in most cases the Li-Cor 6400 (Li-Cor Biosciences, Lincoln, NE, USA), although some measurements were made with the Walz-CMS system (Walz, Effeltrich, Germany). We visually inspected every ACi curve in the dataset for possible outliers and erroneous data points (e.g. negative intercellular CO₂ concentrations). We used criteria based on De Kauwe *et al.* (2016) to screen individual ACi curves for the analysis performed in this paper. Curves were excluded from the analysis if the fitted function (see later) had an r^2 value < 0.99 (however, if the number of replicates available for a given occasion was limited, the threshold r^2 was reduced to 0.90; *c.* 9% of the total number of ACi curves included in the analysis). After screening, the dataset contained a total of 3498 ACi curves measured at leaf temperatures ranging from 1 to 50°C.

Estimating temperature optimum for leaf net photosynthesis (T_{optA})

Ambient leaf net photosynthesis (A_{net}) at each temperature was either obtained from the initial direct measurements at ambient CO₂ concentrations or extracted from the ACi curves. For curves where the first point was not measured at ambient CO₂ concentration, we extracted the A_{net} value at the measured sample CO₂ concentration falling between 300 and 400 ppm. We estimated the temperature optimum for A_{net} , T_{optA} , by fitting a widely used model of instantaneous photosynthetic temperature response (Gunderson *et al.*, 2009; Crous *et al.*, 2013; Sendall *et al.*, 2015; Vårhammar *et al.*, 2015) (Eqn 1) to the net photosynthesis measurements. The model is a quadratic equation, expressed as:

$$A_{\text{net}} = A_{\text{opt}} - b(T - T_{\text{optA}})^2, \quad \text{Eqn 1}$$

where A_{net} is the net photosynthetic rate ($\mu\text{mol m}^{-2} \text{s}^{-1}$) at a given leaf temperature, T (°C), T_{optA} is the temperature

optimum for photosynthesis ($^{\circ}\text{C}$), A_{opt} is the net photosynthetic rate at T_{optA} , and the parameter b (unitless) describes the degree of curvature of the relationship.

Parameterizing biochemical component processes of photosynthesis

We used the FvCB model to characterize photosynthetic biochemical component processes. The model represents leaf net photosynthesis rate as the minimum of three rates: the Rubisco carboxylation limited photosynthetic rate (W_c), the RuBP-regeneration limited photosynthetic rate (W_j), and the triose phosphate utilization limited rate (W_p). The widely used formulation and parameterization of the FvCB model is of the form (Eqns 2–6).

$$A_{\text{net}} = \min(W_c, W_j, W_p) \left(1 - \frac{\Gamma^*}{C_i}\right) - R_L, \quad \text{Eqn 2}$$

$$W_c = V_{\text{cmax}} \frac{C_i}{C_i + K_c \left(1 + \frac{O_i}{K_o}\right)}, \quad \text{Eqn 3}$$

$$W_j = \frac{J}{4} \frac{C_i}{(C_i + 2\Gamma^*)}, \quad \text{Eqn 4}$$

$$W_p = 3\text{TPU}, \quad \text{Eqn 5}$$

where V_{cmax} is the maximum rate of Rubisco activity, C_i and O_i ($\mu\text{mol mol}^{-1}$) are intercellular CO_2 and O_2 concentrations, respectively, K_c and K_o ($\mu\text{mol mol}^{-1}$) are Michaelis–Menten coefficients of Rubisco activity for CO_2 and O_2 respectively, Γ^* ($\mu\text{mol mol}^{-1}$) is the CO_2 compensation point in the absence of photorespiration, TPU ($\mu\text{mol m}^{-2} \text{s}^{-1}$) is the rate of triose phosphate export from the chloroplast, R_L ($\mu\text{mol m}^{-2} \text{s}^{-1}$) is the non-photorespiratory CO_2 evolution in the light, and J ($\mu\text{mol m}^{-2} \text{s}^{-1}$) is the rate of electron transport at a given light intensity. J is related to incident photosynthetically active photon flux density (Q , $\mu\text{mol m}^{-2} \text{s}^{-1}$) by

$$\theta J^2 - (\alpha Q + J_{\text{max}})J + \alpha Q J_{\text{max}} = 0, \quad \text{Eqn 6}$$

where J_{max} ($\mu\text{mol m}^{-2} \text{s}^{-1}$) is the potential rate of electron transport, α ($\mu\text{mol mol}^{-1}$) is the quantum yield of electron transport, and θ (dimensionless) is the curvature of the light response curve (Farquhar *et al.*, 1980; Medlyn *et al.*, 2002a,b; Kattge & Knorr, 2007; Sharkey *et al.*, 2007).

We parameterized Eqns 3–6 using the *fitacis* function within the PLANTECOPHYS package (Duursma, 2015) in R version 3.3.2 (R Development Core Team, 2012). We assumed the Bernacchi *et al.* (2001) kinetic constants for the temperature response of K_c , K_o and Γ^* as given in Medlyn *et al.* (2002a). We used measurement Q in Eqn 6 whenever available (see Table S1); otherwise we assumed a fixed value of $1800 \mu\text{mol m}^{-2} \text{s}^{-1}$. We assumed constant values of α ($0.24 \mu\text{mol mol}^{-1}$) and θ (0.85 (unitless)) for all

datasets (Medlyn *et al.*, 2007); these parameter values have a relatively minor effect on the magnitude of estimated J_{max} (Medlyn *et al.*, 2002a). The estimated parameters, V_{cmax} and J_{max} , are apparent values as we assumed infinite mesophyll conductance (g_m). The significance of g_m for V_{cmax} and J_{max} estimates and their temperature response has been discussed elsewhere (Crous *et al.*, 2013; Bahar *et al.*, 2018). Here, there are insufficient data to quantify g_m and hence it would have been inappropriate to include in our analysis (see Rogers *et al.*, 2017a).

We tested two ACi curve-fitting routines, one with and one without TPU limitation (Eqn 5). Accounting for TPU limitation in the FvCB model did not affect the estimated photosynthetic capacities, apparent V_{cmax} and J_{max} (Fig. S2), suggesting that at ambient CO_2 concentrations, net photosynthesis was rarely limited by TPU (results not shown). Hence, we focused on the temperature responses of apparent V_{cmax} and J_{max} as the principal biochemical components affecting the T_{optA} .

The temperature responses of V_{cmax} and J_{max} were fitted using the peaked Arrhenius function:

$$k_{T_k} = k_{25} \exp \left[\frac{E_a \times 10^3 (T_k - 298.15)}{(298.15 R T_k)} \right] \frac{1 + \exp \left(\frac{298.15 \Delta S - H_d \times 10^3}{298.15 R} \right)}{1 + \exp \left(\frac{T_k \Delta S - H_d \times 10^3}{T_k R} \right)}, \quad \text{Eqn 7}$$

where k_{T_k} is the process rate (i.e. V_{cmax} or J_{max} ; $\mu\text{mol m}^{-2} \text{s}^{-1}$) at a given temperature, T_k (K), k_{25} is the process rate at 25°C , R is the universal gas constant ($8.314 \text{ J mol}^{-1} \text{ K}^{-1}$), and E_a (kJ mol^{-1}) is the activation energy term that describes the exponential increase in enzyme activity with the increase in temperature, H_d (kJ mol^{-1}) is the deactivation energy term that describes, for example, decline in enzyme activity at higher temperature as a result of denaturation of enzymes, and ΔS ($\text{J mol}^{-1} \text{ K}^{-1}$) is the entropy term which characterizes the changes in reaction rate caused by substrate concentration (Johnson *et al.*, 1942). To avoid overparameterization, we assumed a fixed value of 200 kJ mol^{-1} for H_d in Eqn 7 for all species (Dreyer *et al.*, 2001; Medlyn *et al.*, 2002a).

The optimum temperature for k_{T_k} is given by:

$$T_{\text{opt}} = \frac{H_d \times 10^3}{\Delta S - R \ln \left(\frac{E_a}{H_d - E_a} \right)}. \quad \text{Eqn 8}$$

Assessing the contribution of stomatal and respiratory processes

The optimum temperature for photosynthesis is determined by stomatal and respiratory processes as well as biochemical processes (Medlyn *et al.*, 2002a; Lin *et al.*, 2012). Stomatal conductance values are potentially affected by the measurement protocol used in ACi curve measurements which rarely replicates the ambient conditions. Therefore, to assess the relative contribution of stomatal processes to T_{optA} , we calculated the net photosynthesis rate at a fixed C_i of $275 \mu\text{mol mol}^{-1}$ from

each ACi curve, interpolating the curve using the FvCB model with parameters fitted to that curve. A fixed C_i of $275 \mu\text{mol mol}^{-1}$ was chosen, as it roughly corresponds to 70% of ambient $[\text{CO}_2]$. When the photosynthetic rate is scaled to a common C_i , it eliminates the effect of variation in stomatal conductance on photosynthesis, isolating the temperature effects on photosynthetic biochemistry. Similar to net photosynthesis, the temperature optimum for photosynthesis at a fixed C_i ($T_{\text{optA}275}$) was estimated for each species by fitting Eqn 1. We compared $T_{\text{optA}275}$ with T_{optA} to estimate the effect of variation in stomatal conductance on the temperature optimum for photosynthesis.

We fit the standard Arrhenius function (Eqn 9) to R_L values obtained from ACi curves to assess the effect of respiratory component processes on T_{optA} . We estimated two parameters, R_{L25} (R_L at 25°C) and activation energy of R_L (E_a). Similar to J_{max} and V_{cmax} , linear regression was used to test for temperature adaptation and acclimation of R_L .

$$R_L = R_{L25} \exp\left(\frac{E_a \times 10^3 (T_k - 298.15)}{298.15 R T_k}\right), \quad \text{Eqn 9}$$

where R_{L25} is the rate of respiration in light at 25°C .

Test for local adaptation and seasonal temperature acclimation of T_{optA}

We divided the database into three subsets: mature plants growing in their native environments, common-garden datasets, and datasets with seasonal photosynthetic measurements. We used a subset of the data collected in mature plants to identify the patterns in photosynthetic temperature responses of plants in native environments and for model evaluation. Temperature responses in this subset include the effects of both adaptation to the native environment and acclimation to the prevailing temperature. We used the common-garden and seasonal measurements subsets to estimate the relative contributions of adaptation and acclimation, respectively, in determining the observed trends with temperature for plants in native environments.

For plants growing in native environments, we derived relationships between photosynthetic parameters and the prevailing temperature of the growing environment, defined as the mean air temperature for the 30 d before gas exchange measurements (Kattge & Knorr, 2007) (T_{growth}), to identify the temporal trends in photosynthetic temperature responses. We derived T_{growth} using on-site measured real-time daily air temperature for most of the datasets, but for three datasets (Hinoki cypress, Japan; Mongolian oak, Japan; and Scots pine, Finland; Table S1), we extracted T_{growth} values from the original publications, as on-site temperature measurements were not available. We used a general linear model to parameterize the observed responses in the mature plants dataset (Eqn 10)

$$f(T_{\text{growth}}) = a + b T_{\text{growth}}, \quad \text{Eqn 10}$$

where a and b are the intercept and slope, respectively.

Seasonal datasets provide the opportunity to test the acclimation capacity of different species to temporal changes in the ambient temperature of the growing environment. Here, we correlated photosynthetic parameters with growth temperature, T_{growth} , defined as the mean air temperature for the 30 d before gas exchange measurements. Similar to the mature plants dataset, we derived T_{growth} using on-site measured daily air temperature for most of the datasets. For datasets where real-time meteorological data were not available, we extracted T_{growth} values from the original publications.

Common gardens provide an opportunity to test for adaptation, as species with different climates of origin are grown at a common growth temperature. The common-garden datasets included field trials and experiments in controlled environmental conditions, which included two or more species or provenances with contrasting climates of origin. We located the seed source of each species or provenance (latitude and longitude) using published information (Table S1). We used 30'' resolution WorldClim climatology data (WorldClim 1.4; Hijmans *et al.*, 2005) to estimate long-term average (1960–1990) air temperature at seed source. With reference to the species selection criteria used in several common-garden studies (Lin *et al.*, 2013; Vårhammar *et al.*, 2015), we defined mean maximum air temperature of the warmest month at species' seed source as the species' home temperature (T_{home}) and derived relationships between photosynthetic parameters and T_{home} to test for adaptation of species' A_n - T response to climate of origin. We repeated the same analysis with two other forms of species' home temperature – mean growing season air temperature and mean temperature of the warmest quarter – to test whether our results were altered depending on the definition of climate of origin.

For both common-garden and seasonal subsets, we used linear regression against T_{home} and T_{growth} (Eqns 11, 12) to test for temperature adaptation and acclimation, respectively, of T_{optA} , $T_{\text{optA}275}$, the photosynthetic biochemical parameters (V_{cmax} and J_{max}), and their temperature response parameters (see Eqns 7, 8). To test the effect of different biochemical parameters on temperature optimum for photosynthesis, we used linear regression between $T_{\text{optA}275}$ and temperature response parameters of V_{cmax} and J_{max} .

Representing acclimation and adaptation in vegetation models

We derived functions to represent photosynthetic temperature acclimation and adaptation in GVMs. If a given parameter showed only acclimation to growth temperature, the function used was:

$$f(T_{\text{growth}}) = A_{\text{ac}} + \alpha_{\text{ac}} T_{\text{growth}}, \quad \text{Eqn 11}$$

where A_{ac} is the parameter value when $T_{\text{growth}} = 0$ and α_{ac} is the acclimation coefficient ($^\circ\text{C}^{-1}$).

If a parameter showed only adaptation to climate of origin, the function was:

$$f(T_{\text{home}}) = A_{\text{ad}} + \alpha_{\text{ad}} T_{\text{home}}. \quad \text{Eqn 12}$$

We combined Eqns 11 and 12 to represent both acclimation and adaptation, defined as

$$f(T_{\text{home}}, T_{\text{growth}}) = A_{\text{ad}} + \alpha_{\text{ad}} T_{\text{home}} + \delta_{\text{ac}}(T_{\text{growth}} - T_{\text{home}}), \quad \text{Eqn 13}$$

where, δ_{ac} is the acclimation coefficient corresponding to a unit deviation in T_{growth} from the species' T_{home} ($^{\circ}\text{C}^{-1}$). We parameterized Eqns 11 and 12 independently using data from seasonal photosynthetic response studies (Eqn 11) and common-garden experiments (Eqn 12). Eqn 13 was parameterized using combined seasonal and common-garden datasets. We implemented the modified functions into the FvCB model (see Duursma, 2015) to simulate photosynthetic temperature response curves at a constant C_i of $275 \mu\text{mol mol}^{-1}$ and tested how well the leaf-scale photosynthesis model captured the observed temperature optimum of photosynthesis in the mature plants dataset. This provided an independent comparison, as the mature plants dataset was not used to parameterize the temperature acclimation and adaptation functions (Eqns 11–13).

Statistical analysis

Parameters of Eqns 1, 7–9 were estimated in a nonlinear mixed model framework (Zuur *et al.*, 2009) using the *nlme* function within the NLME package in R v.3.3.2 (R Development Core Team, 2012). Replicate trees and/or leaves of the same species were included as random effects. However, when datasets contained measurements of multiple species (e.g. Brazilian rainforests, Australian rainforests and Australian semiarid woodland datasets; Table S1), individual species were considered as a random variable in the model. Similarly, Eqns 11–13 were parameterized in a linear mixed model framework using the inverse of the standard error (SE) of each parameter of Eqns 1, 7–9 as the weighting scale to account for parameter uncertainty (Zuur *et al.*, 2009; Lin *et al.*, 2015). We tested whether the model parameters (Eqns 11–13) differed significantly among datasets (and/or species) by fitting linear mixed models with and without random slopes and intercepts for each dataset (and or species). These models were then compared using a likelihood ratio test (Zuur *et al.*, 2009) to determine whether the acclimation and adaptation coefficients differed among species. We used standard model validation tools (normal quantile plots and residual plots) to test the underlying assumptions in linear mixed models, and marginal and conditional r^2 values to evaluate the goodness of fit (Nakagawa & Schielzeth, 2013). The complete database used for this analysis is available as a public data product (Kumarathunge *et al.*, 2018) and the code used for the entire analysis is publicly available through <https://bitbucket.org/Kumarathunge/photom>.

Results

Temperature optimum for net photosynthesis at saturating irradiance (T_{optA})

The temperature optimum for leaf-level net photosynthesis at saturating irradiance (T_{optA}) of mature plants in their natural

habitats was strongly correlated with the temperature of the growth environment (T_{growth} ; mean air temperature of preceding 30 d; Fig. 1a; Table 1). Values of T_{optA} ranged from 16.3 to 32.4 $^{\circ}\text{C}$, where the minimum and maximum values were observed for Arctic vegetation and tropical evergreen trees, respectively. The rate of increase in T_{optA} was $0.62 \pm 0.07^{\circ}\text{C}$ per $^{\circ}\text{C}$ increase in T_{growth} .

In the seasonal dataset (Fig. 1b), we found strong evidence for acclimation of T_{optA} to the prevailing growth temperature. T_{optA} showed a significant increasing trend with T_{growth} . The mean rate of increase in T_{optA} was $0.34 \pm 0.05^{\circ}\text{C}$ per unit increase in T_{growth} (Table 1). By contrast, no trend was observed with climate of origin in common-garden studies (Table 1). Here, we tested for a relationship between T_{optA} and the T_{home} (1960–1990 mean maximum air temperature of the warmest month at species' seed source) and we did not find any significant relationship for T_{optA} with T_{home} (Fig. 1c; Table 1). The results were similar for the two alternative definitions of the climate of origin (Table S2). The lack of a significant relationship with the species' home temperature in the common-garden datasets suggests that the variation in T_{optA} of mature plants across ecosystems (Fig. 1a) is more strongly driven by acclimation to growth temperatures (Fig. 1b) than by local adaptation to climate of origin (Fig. 1c).

Temperature optimum for photosynthesis at a common C_i (T_{optA275})

Similar to T_{optA} , T_{optA275} showed a strong correlation with T_{growth} in mature plants across ecosystems (Fig. 1d; Table 1). We found no significant differences in either intercept or slope of the linear regression between T_{optA} and T_{optA275} vs T_{growth} (Table 1), in both the mature (Fig. 1a,d) and seasonal (Fig. 1b,e) datasets, strongly suggesting that the observed variation in T_{optA} among ecosystems is not a result of variation in the stomatal limitation of T_{optA} . This result also suggests that the observed seasonal pattern of T_{optA} (Fig. 1b) was not driven by stomatal processes but rather by the effects of photosynthetic biochemical processes. Similar to T_{optA} , species in common-garden studies did not show significant trends for T_{optA275} with T_{home} (Fig. 1f).

Temperature dependence of biochemical capacities, J_{max} and V_{cmax}

Similar to T_{optA} , we found a strong increase in both T_{optV} and T_{optJ} with T_{growth} in the mature plants dataset (Fig. 2a,d). The slopes of the linear regression with T_{growth} were similar for T_{optV} and T_{optJ} (0.71 ± 0.20 and $0.63 \pm 0.15^{\circ}\text{C } ^{\circ}\text{C}^{-1}$, respectively). These sensitivities are similar in magnitude to the sensitivity of T_{optA} and T_{optA275} to T_{growth} in the mature plants dataset. For V_{cmax} , the trend in T_{opt} was caused by an increase ($P \approx 0.06$) in E_{aV} with increasing T_{growth} , and a strong decline in ΔS_V (Fig. 2b, c). For J_{max} , however, there was no change in E_{aJ} , only a decline in ΔS_J with increasing T_{growth} (Fig. 2e,f).

We decomposed the observed trends across biomes shown in Fig. 2 by looking at seasonal datasets (Fig. 3) and common-

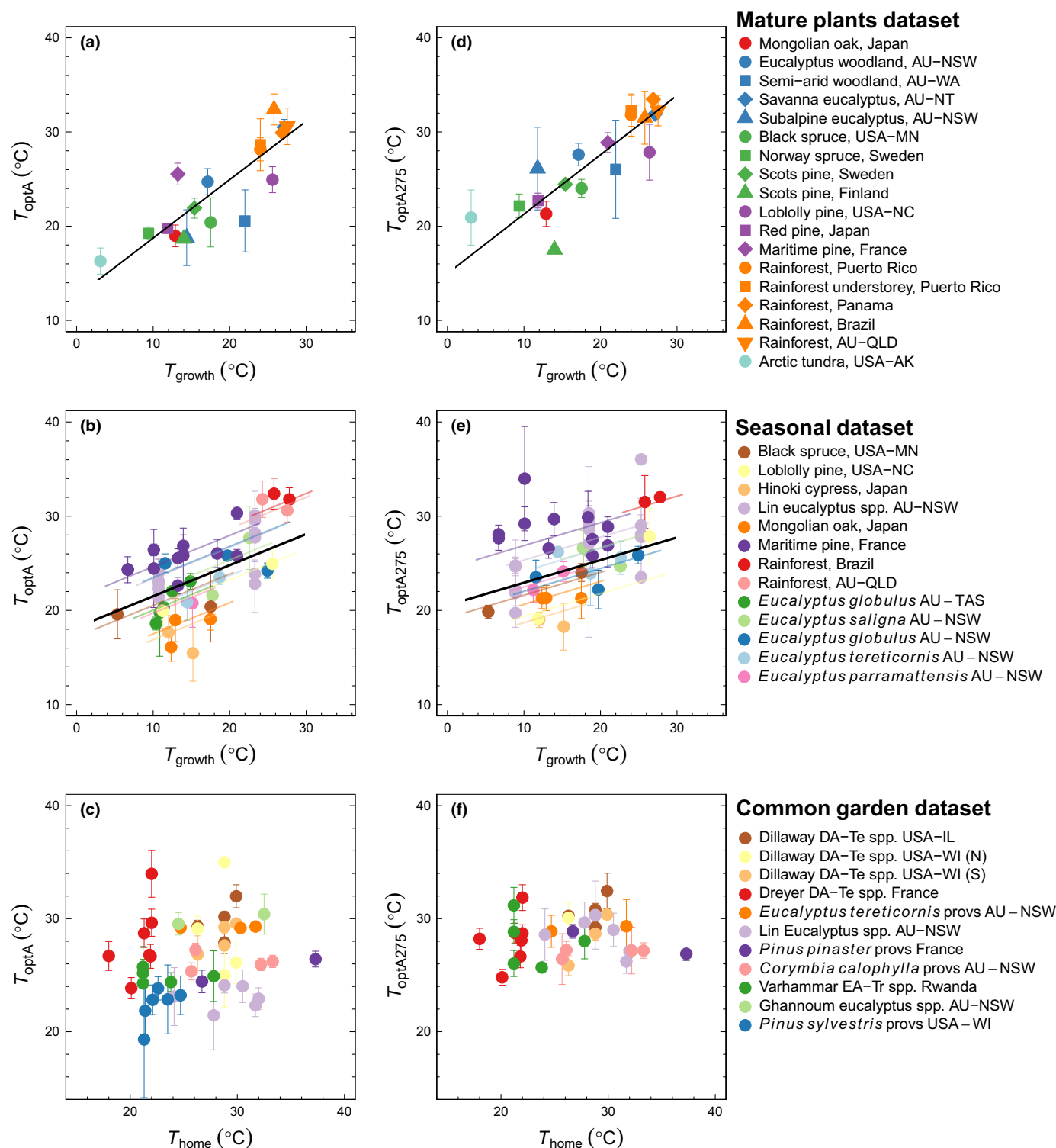


Fig. 1 Temperature optimum for leaf net photosynthesis (T_{optA}) (a–c) and net photosynthesis at an intercellular CO_2 concentration of $275 \mu\text{mol mol}^{-1}$ ($T_{\text{optA}275}$) (d–f) of mature plants growing in their native environments (a, d), species in the field (grown at ambient growth temperatures) measured in at least two or more seasons (b, e) and species or provenances from contrasting climates of origin grown in common growth temperatures (common gardens or controlled environments) (c, f). T_{growth} , mean air temperature of the preceding 30 d; T_{home} , long-term (1960–1990) mean maximum temperature of the warmest month at species' seed origin. Different colours in (a, d) depict plant functional types: orange, tropical evergreen angiosperms (EA-Tr); light blue, arctic tundra; red, temperate deciduous angiosperms (DA-Te); blue, temperate evergreen angiosperms (EA-Te); green, boreal evergreen gymnosperms (EG-Br); purple, temperate evergreen gymnosperms (EG-Te); those in (b, c, e, f) depict different datasets. The thick black lines are: (a, d) least-squares linear regression fits; (b, c, e, f) linear mixed-effect model fits with random intercepts for each dataset. The thin lines in respective colours are the fitted random intercept models for individual datasets. Error bars represent ± 1 SE.

Table 1 Results of the linear regression analysis of the parameters of Eqns 1, 7–9.

Mature plants in native environment (Eqn 10)					Seasonal dataset (Eqn 11)				Common-garden dataset (Eqn 12)					
Parameter	<i>a</i>	<i>b</i>	<i>r</i> ²	<i>P</i> -value	<i>A</i> _{ac}	<i>α</i> _{ac}	<i>r</i> ² (marginal)	<i>r</i> ² (conditional)	<i>P</i> -value	<i>A</i> _{ad}	<i>α</i> _{ad}	<i>r</i> ² (marginal)	<i>r</i> ² (conditional)	<i>P</i> -value
Biochemical parameters														
<i>T</i> _{optA}	12.5 (1.4)	0.62 (0.1)	0.80	<0.001	18.2 (1.1)	0.34 (0.05)	0.27	0.87	<0.001	24.8 (2.1)	0.07 (0.1)	0.01	0.71	0.309
<i>T</i> _{optA275}	14.9 (1.5)	0.63 (0.1)	0.84	<0.001	20.5 (1.2)	0.24 (0.05)	0.16	0.85	<0.001	26.8 (2.3)	0.07 (0.1)	0.03	0.30	0.400
Respiratory parameters														
<i>V</i> _{cmx25}	85.3 (16.7)	−1.84 (0.8)	0.19	0.404	58.2 (12.0)	0.50 (0.4)	0.01	0.94	0.252	33.4 (28.0)	1.62 (0.9)	0.07	0.91	0.096
<i>J</i> _{max25}	194.7 (24.1)	−5.13 (1.2)	0.53	<0.001	141.3 (18.8)	−1.35 (0.7)	0.03	0.95	0.053	92.7 (47.2)	1.63 (1.6)	0.02	0.95	0.312
<i>E</i> _{av}	48.7 (7.8)	0.82 (0.4)	0.14	0.067	39.7 (6.2)	1.14 (0.3)	0.32	0.91	<0.001	79.4 (13.1)	−0.37 (0.5)	0.14	0.14	0.450
<i>E</i> _{al}	43.5 (9.8)	−0.19 (0.5)	0.05	0.7143	27.2 (5.0)	0.26 (0.3)	0.04	0.82	0.325	51.5 (8.7)	−0.38 (0.3)	0.20	0.20	0.247
<i>ΔS</i> _v	662.0 (8.7)	−1.31 (0.5)	0.30	0.011	645.1 (4.6)	−0.38 (0.2)	0.09	0.82	0.089	647.9 (9.5)	−0.36 (0.3)	0.08	0.66	0.302
<i>ΔS</i> _j	667.3 (7.8)	−1.34 (0.4)	0.36	0.005	653.9 (4.6)	−0.85 (0.2)	0.22	0.94	<0.001	662.3 (7.5)	−0.99 (0.3)	0.49	0.84	<0.001
<i>T</i> _{optV}	24.3 (3.8)	0.71 (0.2)	0.40	0.002	30.3 (1.9)	0.36 (0.1)	0.23	0.77	<0.001	34.3 (3.3)	0.12 (0.1)	0.05	0.36	0.335
<i>T</i> _{optU}	19.9 (2.9)	0.63 (0.2)	0.52	<0.001	27.6 (1.8)	0.31 (0.1)	0.13	0.91	<0.001	24.8 (3.4)	0.42 (0.1)	0.42	0.60	<0.001
<i>JV</i> _r	2.9 (0.2)	−0.06 (0.01)	0.66	<0.001	2.3 (0.2)	−0.03 (0.01)	0.07	0.17	<0.001	2.5 (0.3)	−0.03 (0.01)	0.13	0.64	0.005
Biochemical parameters														
<i>R</i> _{L25}	2.8 (0.5)	−0.09 (0.03)	0.38	0.0037	1.54 (0.42)	−0.01 (0.02)	0.01	0.25	0.502	1.16 (0.45)	0.01 (0.01)	0.01	0.61	0.583
<i>E</i> _a	−20.7 (14.3)	1.18 (0.78)	0.07	0.1508	−9.17 (11.49)	0.42 (0.61)	0.02	0.83	0.485	−4.25 (43.38)	0.12 (1.57)	0.01	0.93	0.937
<i>R</i> _{L25} :	0.036	−0.001	0.22	0.033	0.03 (0.01)	−0.001	0.04	0.60	0.043	0.03 (0.01)	−0.0005	0.06	0.53	0.149
<i>V</i> _{cmx25}	(0.01)	(0.0003)			(0.0003)	(0.0003)					(0.0004)			

For common-garden and seasonal datasets, linear mixed models were fitted accounting for between-dataset variations of a given parameter (see the Materials and Methods section for details). For mature plants in native environments, parameter values were derived by fitting simple linear regression models (Eqn 10). Values in parentheses are standard errors of estimates. Bold values are the significant parameters at $\alpha = 0.05$. V_{cmx25} , maximum rate of Rubisco activity (V_{cmx}) at a standard temperature of 25°C; J_{max25} , potential rate of electron transport (J_{max}) at a standard temperature of 25°C; JV_r , ratio $J_{max25} : V_{cmx25}$; E_{av} , activation energy of J_{max} ; E_{al} , activation energy of V_{cmx} ; ΔS_v , entropy of V_{cmx} ; ΔS_j , entropy of J_{max} ; T_{optV} , optimum temperature of V_{cmx} ; T_{optU} , optimum temperature of J_{max} ; R_{L25} , non-photorespiratory CO_2 evolution in the light at a standard temperature of 25°C; E_a , activation energy of RL.

garden studies (Fig. 4) independently to identify the effect of seasonal acclimation and local adaptation of photosynthetic biochemical component processes. We found a strong increase in T_{optV} and T_{optJ} with T_{growth} (Fig. 3a,d). The rate of increase in T_{optJ} per unit increase in T_{growth} was slightly higher than that in T_{optV} (Table 1), but the difference was not significant. Further, these sensitivities were found to be similar to the sensitivity of both T_{optA} and T_{optA275} to T_{growth} . Similar to the mature plants dataset, we found a significant positive trend for E_{aV} and a decreasing trend ($P \approx 0.08$) for ΔS_{V} with increasing T_{growth} (Fig. 3b,c). For J_{max} , however, there was no change in E_{aJ} , only a strong decline in ΔS_{J} with increasing T_{growth} (Fig. 3e,f).

We found no evidence to support adaptation of T_{optV} , E_{aV} and ΔS_{V} to climate of origin as there were no significant trends observed with temperature at species' seed source (i.e. T_{home}) in the common-garden dataset (Fig. 4a–c). These observations were consistent with the lack of significant trends for T_{optA} in the common-garden dataset. However, T_{optJ} and ΔS_{J} showed significant

trends with T_{home} (Fig. 4d–f; Table 1), suggesting the adaptation of both parameters to climate of origin. The results were similar for the two alternative definitions of the climate of origin (Table S2).

The balance between J_{max} and V_{cmax}

We found no detectable correlation between T_{growth} and the basal rate of V_{cmax} at a standard temperature 25°C for mature plants in their natural habitats, but the basal rate of J_{max} showed a strong decrease (Fig. 5a,b). The ratio of $J_{\text{max}} : V_{\text{cmax}}$ at 25°C (JV_r) showed a significant decrease with increasing T_{growth} (Fig. 5c, Table 1). We excluded the Scots pine, Finland dataset when fitting linear regression, as the JV_r value departed significantly from the general trend and was therefore identified as an outlier (black circle in Fig. 5c).

Basal rates of V_{cmax} and J_{max} did not show significant trends with T_{growth} , but JV_r responded negatively to T_{growth} in the seasonal dataset (Fig. 5d,f). We found no evidence to support

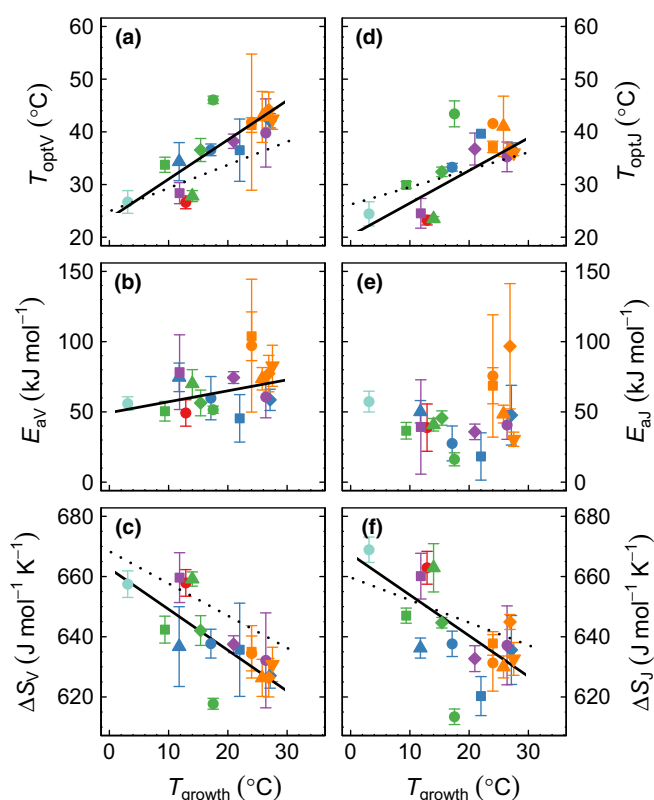


Fig. 2 Biochemical temperature response parameters for the mature plants dataset in relation to mean air temperature of the preceding 30 d (T_{growth}). Different colours represent plant functional types as in Fig. 1(a, d). Solid and dotted lines in each panel are the least-squares linear regression fits (this study; coefficients and r^2 -values given in Table 1) and the linear models proposed by Kattge & Knorr (2007), respectively. Error bars represent ± 1 SE. Legend follows Fig. 1(a, d). E_{aV} , activation energy of the maximum rate of Rubisco activity (V_{cmax}); E_{aJ} , activation energy of the maximum potential electron transport rate (J_{max}); T_{optV} , optimum temperature of V_{cmax} ; T_{optJ} , optimum temperature of J_{max} ; ΔS_{V} , entropy of V_{cmax} ; ΔS_{J} , entropy of J_{max} .

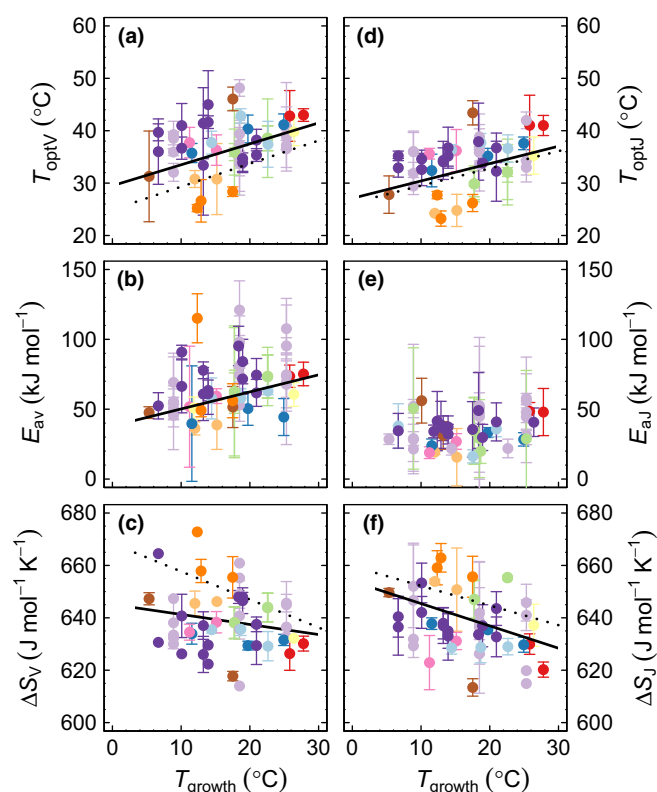


Fig. 3 Biochemical temperature response parameters for the seasonal dataset in relation to mean air temperature of the preceding 30 d (T_{growth}). Data were measured on field-grown plants (including whole-tree chamber experiments) in two or more seasons. Solid and dotted lines in each panel are the linear mixed-effect model fits (this study; coefficients and r^2 -values are given in Table 1) and the linear models proposed by Kattge & Knorr (2007), respectively. Error bars represent ± 1 SE. E_{aV} , activation energy of the maximum rate of Rubisco activity (V_{cmax}); E_{aJ} , activation energy of the potential rate of electron transport (J_{max}); T_{optV} , optimum temperature of V_{cmax} ; T_{optJ} , optimum temperature of J_{max} ; ΔS_{V} , entropy of V_{cmax} ; ΔS_{J} , entropy of J_{max} . Legend follows Fig. 1(b, e).

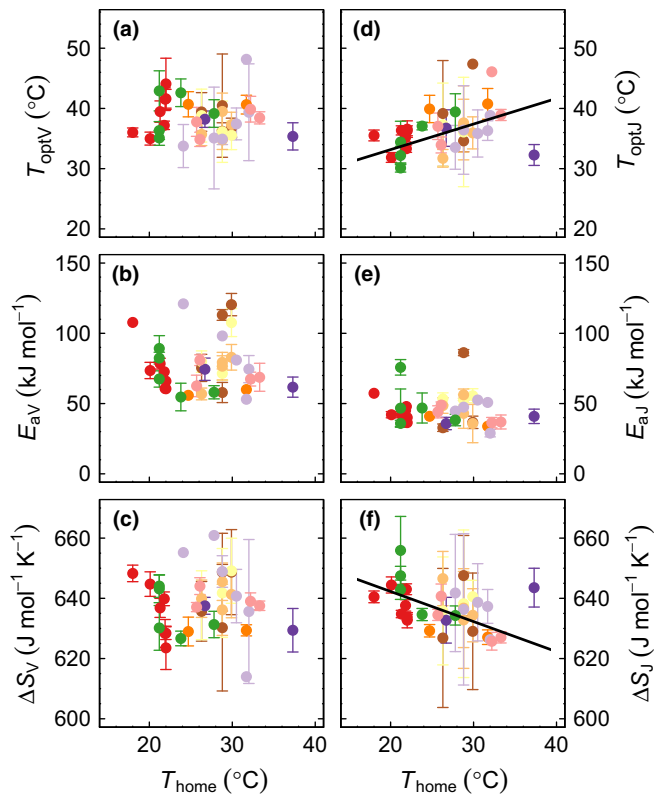


Fig. 4 Biochemical temperature response parameters for the common-garden dataset in relation to the long-term (1960–1990) mean maximum temperature of the warmest month at species' seed origin (T_{home}). Data were measured in species or provenances from contrasting climates of origin grown at common growth temperatures (common gardens and controlled environments). Solid lines in each panel are the linear mixed-effect model fits (this study; coefficients and r^2 -values are given in Table 1). Error bars represent ± 1 SE. E_{aV} , activation energy of the maximum rate of Rubisco activity (V_{cmax}); E_{aJ} , activation energy of the potential rate of electron transport (J_{max}); T_{optV} , optimum temperature of V_{cmax} ; T_{optJ} , optimum temperature of J_{max} ; ΔS_V , entropy of V_{cmax} ; ΔS_J , entropy of J_{max} . Legend follows Fig. 1(c, f).

adaptation of basal rates of V_{cmax} and J_{max} to climate of origin; no parameters showed any significant trend with T_{home} in the common-garden dataset (Fig. 5g,h; Table 1). However, there was evidence of adaptation of JV_r to climate of origin, as JV_r showed a significant decrease with T_{home} in the common-garden dataset (Fig. 5I; Table 1).

Assessing the role of day respiration

We found no detectable trends (Fig. S3; Table 1) for either R_{L25} or E_a of mature plants in native environments. Similar results were found for common-garden studies and no seasonal trends were observed for either R_{L25} or E_a in the seasonal dataset. However, the data showed a slight negative trend for $R_{L25} : V_{\text{cmax}25}$ ratio with increasing T_{growth} (of mature plants in native environments) and T_{growth} (of seasonal datasets) (Fig. S4). We also observed negative E_a values in all three datasets (Fig. S4).

Model to represent acclimation and adaptation in vegetation models

Our results provide evidence that changes in the temperature response of photosynthesis among datasets are principally driven by acclimation of photosynthetic biochemistry to growth temperature. Both E_{aV} and JV_r showed strong acclimation to growth temperature with significant (albeit weak) acclimation of ΔS_V . We found little evidence to support local adaptation of photosynthetic biochemistry to climate of origin. Only JV_r and ΔS_J showed statistically significant, but weak, signals of local adaptation. We further tested whether variation in E_{aV} and JV_r can explain the seasonal acclimation of temperature optimum of photosynthesis observed in the seasonal dataset using linear regression analysis (JV_r and E_{aV} vs $T_{\text{optA}275}$). We found a strong negative trend for the relationship between JV_r and $T_{\text{optA}275}$ (Fig. 6a). $T_{\text{optA}275}$ increased by $c. 6^\circ\text{C}$ for a unit decrease in JV_r . Also, we found a significant trend between E_{aV} and $T_{\text{optA}275}$; $T_{\text{optA}275}$ increased by $c. 0.2^\circ\text{C}$ for a unit increase in E_{aV} (Fig. 6b). Therefore, the observed trends in T_{optA} of mature plants in native habitats (Fig. 1a) can be explained by the effect of growth temperature on E_{aV} , ΔS_V and JV_r and the effects of both growth temperature and climate of origin on ΔS_J and JV_r . Hence, photosynthetic temperature acclimation and adaptation can be implemented in GVMs using these parameters. Therefore, we modified the baseline peaked Arrhenius functions (Eqn 8) to represent temporal variability of E_{aV} and ΔS_V using Eqn 12, and geographical and temporal variation of the JV_r ratio at 25°C and ΔS_J using Eqn 13. The full final model is given in Table 2.

We found that the new temperature response functions were able to predict the temperature optima of photosynthesis observed in field-grown mature plants with a high degree of accuracy ($r^2 = 0.80$). The slope (1.09 ± 0.15) and intercept (-2.20 ± 4.10) of the linear regression between the predicted and observed T_{optA} were not significantly different from unity and zero, respectively (Fig. 7a; Table S3). Our new model outperformed the Kattge & Knorr (2007) algorithms, which tend to underpredict T_{optA} (Fig. 7b; Table S3). Further, the use of PFT-specific values of V_{cmax} , together with a standard unacclimated photosynthetic temperature responses (Leuning, 2002), was not able to predict the observed variability in T_{optA} , as it predicts a $T_{\text{optA}} \approx 25^\circ\text{C}$ for all datasets (Fig. 7a). Note that the mature plant dataset was not included in fitting Eqns 11–13, so that the predicted $T_{\text{optA}275}$ in Fig. 7(a) was independent of the data used to derive the model parameters.

Discussion

We developed new mathematical functions to represent the photosynthetic temperature response in vegetation models to account for both acclimation to growth temperature and adaptation to climate of origin using a global database that contains > 140 species. We found acclimation to growth temperature to be the principal driver of the photosynthetic temperature response, and observed only a few modest effects of adaptation to temperature at the climate of origin. The observed variation of temperature

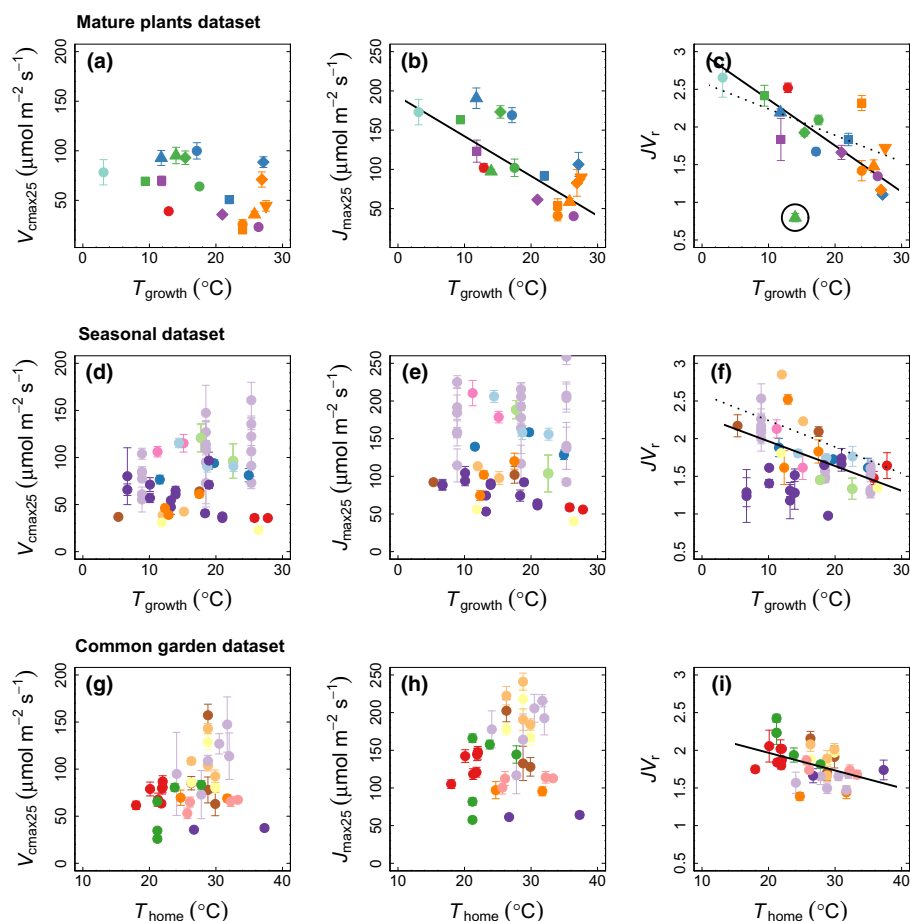


Fig. 5 Maximum rate of Rubisco activity (V_{cmax}), potential rate of electron transport (J_{max}) and $J_{max} : V_{cmax}$ ratio (JV_r) at a standard leaf temperature (25°C) of: (a–c) mature plants growing in their native environments; (d–f) field-grown plants measured in two or more seasons; and (g–i) species or provenances from contrasting climates of origin grown in common growth temperatures (common gardens or controlled environments). T_{growth} , mean air temperature of preceding 30 d; T_{home} , long-term (1960–1990) mean maximum temperature of the warmest month at species' seed origin, respectively. Solid lines in each panel are the least-squares linear regression fits (b, c), and linear mixed-effect model fits with random intercepts for each dataset (f, i). One outlier is circled in (c) (see the Results section). Error bars represent ± 1 SE. Legend follows Fig. 1.

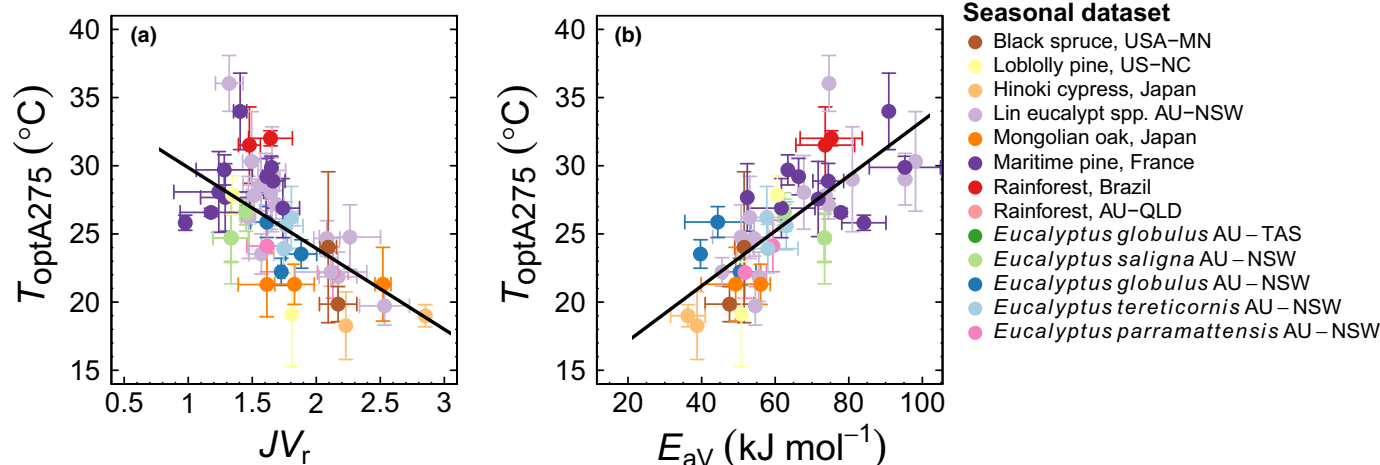


Fig. 6 Relationship between potential rate of electron transport (J_{max}) : maximum rate of Rubisco activity (V_{cmax}) ratio (JV_r) at a standard leaf temperature (25°C) and temperature optimum for photosynthesis at a fixed intercellular CO_2 concentration of $275 \mu\text{mol mol}^{-1}$ ($T_{optA275}$) (a) and relationship between activation energy of V_{cmax} (E_{av}) and $T_{optA275}$ (b). Data were measured on field-grown plants (including whole-tree chamber experiments) in two or more seasons. Lines in each panel are the linear mixed effect regression model fits (a, $T_{optA275} = 35.78 - 5.93 \times JV_r$, $R^2 = 0.36$; b, $T_{optA275} = 13.11 + 0.20 \times E_{av}$, $R^2 = 0.49$). Error bars represents ± 1 SE.

optimum for leaf net photosynthesis was primarily explained by the photosynthetic biochemical component processes rather than stomatal or respiratory processes. The new temperature response

functions presented here capture the observed T_{optA} across biomes with higher degree of accuracy than previously proposed algorithms.

Table 2 Parameters of the temperature acclimation and adaptation functions developed in this study.

Parameter	Model representation	Value	Units
$V_{\text{cmax}25}$	PFT specific	DA-Te	39.0
		EA-Te	82.9
		EG-Te	42.8
		EG-Br	80.4
		EA-Tr	39.4
		Arctic tundra	78.3
$J_{\text{max}25}$	Acclimation + adaptation	$V_{\text{cmax}25} \times J_V$	$\mu\text{mol m}^{-2} \text{s}^{-1}$
J_V	Acclimation + adaptation	$2.56 - 0.0375 T_{\text{home}} - 0.0202 (T_{\text{growth}} - T_{\text{home}})$	Unitless
E_{aV}	Acclimation	$42.6 + 1.14 T_{\text{growth}}$	kJ mol^{-1}
E_{aJ}	Global mean	40.71	kJ mol^{-1}
ΔS_V	Acclimation	$645.13 - 0.38 T_{\text{growth}}$	$\text{J mol}^{-1} \text{K}^{-1}$
ΔS_J	Acclimation + adaptation	$658.77 - 0.84 T_{\text{home}} - 0.52 (T_{\text{growth}} - T_{\text{home}})$	$\text{J mol}^{-1} \text{K}^{-1}$

T_{home} , long-term (1960–1990) mean maximum temperature of the warmest month; T_{growth} , mean air temperature of preceding 30 d. Plant functional types (PFTs): DA-Te, temperate deciduous angiosperms; EA-Te, temperate evergreen angiosperms; EG-Te, temperate evergreen gymnosperms; EG-Br, boreal evergreen gymnosperms; EA-Tr, tropical evergreen angiosperms; Arctic tundra, Arctic spp.; $V_{\text{cmax}25}$, maximum rate of Rubisco activity (V_{cmax}) at a standard temperature of 25°C; $J_{\text{max}25}$, potential rate of electron transport electron transport rate (J_{max}) at a standard temperature of 25°C; J_V , ratio $J_{\text{max}25} : V_{\text{cmax}25}$; E_{aV} , activation energy of V_{cmax} ; E_{aJ} , activation energy of J_{max} ; ΔS_V , entropy of V_{cmax} ; ΔS_J , entropy of J_{max} .

Adaptation of T_{optA} to climate of origin

Despite a significant range in long-term mean temperature at species' seed sources, we found no predictable relationship for T_{optA} with climate of origin when species were grown in common gardens. Therefore, our results do not support the hypothesis that T_{optA} is adapted to species' climate of origin (hypothesis 1). Our results contrast with previous studies which found that T_{optA} is related to species climate of origin (Fryer & Ledig, 1972; Slatyer, 1977, 1978; Robakowski *et al.*, 2012), but there are a number of studies which compare the temperature response of photosynthesis and report a lack of local adaptation of T_{optA} (Ledig & Korbobo, 1983; Gunderson *et al.*, 2000). We propose two hypotheses to explain the lack of local adaptation of T_{optA} : there is a lack of specialization in photosynthetic biochemistry in relation to climate of origin; and the capacity of species to adjust their T_{optA} to temporal variations in local thermal environment could mask ecotypic thermal adaptation of T_{optA} (Robakowski *et al.*, 2012).

With respect to the first hypothesis, Rubisco activity is one of the key photosynthetic biochemical determinants and one of the most temperature-responsive physiological process (Galmés *et al.*, 2015). Several lines of evidence suggest that Rubisco catalytic properties, including the relative specificity for CO_2/O_2 ($S_{\text{c/o}}$), the Michaelis–Menten constants for CO_2 (K_{c}) and O_2 (K_{o}), and the maximum turnover of carboxylation (k_{c}), differ among

species that have evolved under different thermal environments (Andersson & Backlund, 2008; Galmés *et al.*, 2014). However, it is not clear whether these differential responses are a result of genetic adaptation of Rubisco kinetics to climate of origin or to the temporal effects of growth temperature. Galmés *et al.* (2015) argued that closely related species could be less adapted to their current thermal environment as a result of past strategies that limit adaptation of Rubisco to new thermal regimes (Lambers *et al.*, 2008). This hypothesis was further supported by Savir *et al.* (2010), who suggested that point mutations may not cause a significant improvement in Rubisco activity owing to its close optimality in the net photosynthetic rate (Tcherkez *et al.*, 2006). As a result, the adaptive evolution of Rubisco to novel thermal environments may be rare, as adaptation to a local environment will be working against the selective pressure to cope with seasonal and annual temperature variations and would reduce species fitness and expansion into new niches with different thermal environments. Other than the parameters ΔS_J and J_V , our results do not show evidence of thermal adaptation of photosynthetic biochemical parameters. Thus we suggest that the lack of local adaptation of T_{optA} may be partially explained by the lack of specialization in photosynthetic biochemistry, particularly Rubisco kinetic properties to species climate of origin.

Regarding the second hypothesis, we suggest that the capacity of Rubisco kinetic properties to adjust to temporal variations in growth temperature could potentially mask the species' preadaptive responses to their original thermal environments. Here, we show strong evidence for the acclimation of T_{optA} to species T_{growth} , which is primarily a result of the variations in photosynthetic biochemical component processes J_V , E_{aV} , ΔS_V and ΔS_J in relation to the seasonal temperature dynamics. Potential mechanisms by which the kinetic properties of Rubisco could be altered in response to changes in temperature include structural changes in the Rubisco enzyme itself (Huner & Macdowall, 1979; Huner, 1985; Yamori *et al.*, 2006); changes in the concentration of other photosynthetic enzymes such as Rubisco activase (Yamori *et al.*, 2005, 2011); expression of cold/heat-stable isozymes (Yamori *et al.*, 2006); and alterations in membrane fluidity (Falcone *et al.*, 2004). A number of previous studies have demonstrated short-term acclimation of Rubisco kinetics to growth temperature (Medlyn *et al.*, 2002b; Yamori *et al.*, 2006; Kattge & Knorr, 2007; Lin *et al.*, 2013; Yamaguchi *et al.*, 2016; Smith & Dukes, 2017; Crous *et al.*, 2018), although the sensitivities of the responses varied. In addition, studies that have compared the acclimation capacity of multiple species in common growth temperatures have shown similar direction and magnitude of short-term temperature acclimation of T_{optA} (Berry & Björkman, 1980; Sendall *et al.*, 2015) and Rubisco kinetics (Lin *et al.*, 2013; Smith & Dukes, 2017) across species irrespective of their climate of origin. Therefore, we argue that the capacity of species to adjust their photosynthetic biochemistry to temporal variations in growth temperature provides a fitness advantage over that of local climatic adaptation of T_{optA} and its related mechanisms, by enabling species to optimize C balance in their current habitat (Hikosaka *et al.*, 2006).

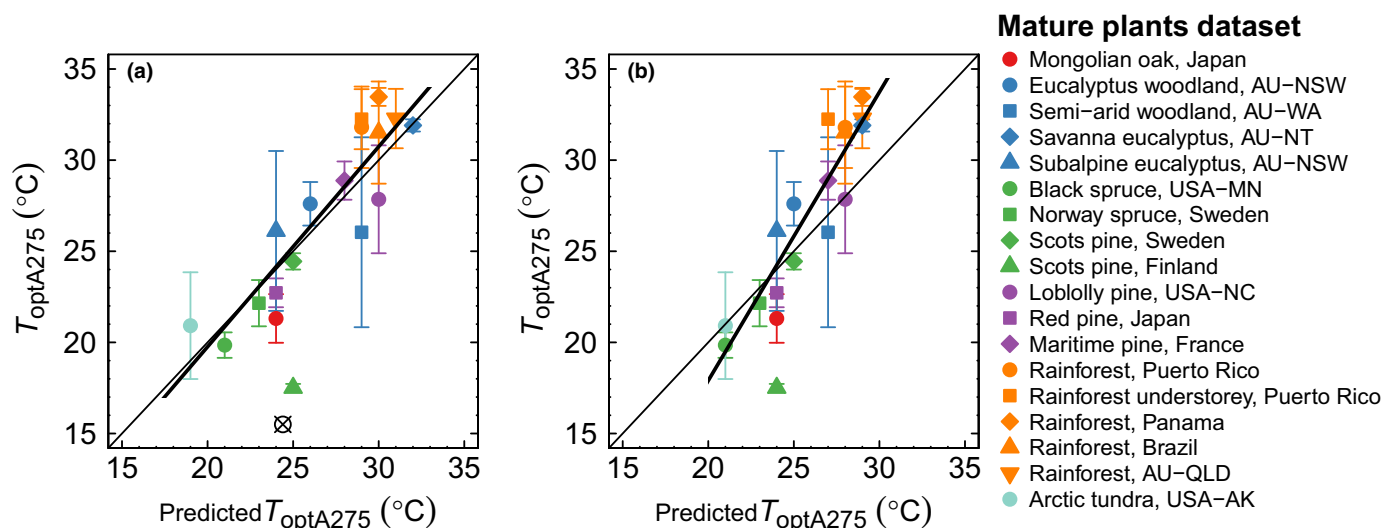


Fig. 7 Observed and predicted temperature optimum for photosynthesis at a fixed intercellular CO_2 concentration (C_i) of $275 \mu\text{mol mol}^{-1}$ using model parameterizations given in Table 2. (a) With acclimation and adaptation functions developed in this study ($y = 1.09x - 2.20$, $r^2 = 0.80$); (b) Kattge & Knorr (2007) acclimation function ($y = 1.58x - 13.82$, $r^2 = 0.83$). The crossed circle in the x-axis of (a) depicts the predicted temperature optimum for photosynthesis at a fixed intercellular CO_2 concentration of $275 \mu\text{mol mol}^{-1}$ ($T_{\text{optA}275}$) with a fixed set of parameters without acclimation and adaptation (Leuning, 2002). Colours reflect plant functional types as in Fig. 1. Thin lines, 1 : 1 relationship; thick lines, least-squares regression fit. In (a), the intercepts and the slope of the linear regression were not significantly different from zero and unity respectively (Supporting Information Table S3). Error bars represent ± 1 SE.

The lack of a temperature adaptation response in this study contrasts with the results of a previous meta-analysis which found both evolutionary changes and an acclimation effect on T_{optA} (Yamori *et al.*, 2014). Our common-garden studies compared closely related species (or provenances of the same species) in most cases. The most climatically divergent sets of species included in this study were those of Vårhammar *et al.* (2015) (lowland and montane tropical species) and Dillaway & Kruger (2010) (North American boreal and temperate deciduous species; see Table S1). By contrast, Yamori *et al.* (2014) compared temperature responses of C_3 , C_4 and CAM plants and found evidence of evolutionary shifts among these functional groups. Other common-garden studies with taxonomically diverse species have also provided evidence of evolutionary changes in T_{optA} in relation to climate of origin (Cunningham & Read, 2002; Reich *et al.*, 2015).

Acclimation of T_{optA} to growth temperature

Our observations of seasonal photosynthetic temperature response datasets suggest that the seasonal plasticity in T_{optA} is principally driven by the adjustment of the temperature response of the Rubisco-limited photosynthetic rate and the balance between Rubisco-limited and electron transport-limited photosynthetic rates. These two mechanisms control the seasonal shifts in T_{optA} as follows. First, at biologically relevant leaf temperatures, the light-saturated net photosynthetic rate is mostly limited by Rubisco activity (Rogers & Humphries, 2000; De Kauwe *et al.*, 2016; Yamaguchi *et al.*, 2016). An increase in E_{aV} along with a decrease in ΔS_V increases the Rubisco-limited photosynthetic rate with temperature, and thus affects the shape of the photosynthetic temperature response. The rate of increase in E_{aV} with T_{growth} in this study ($1.14 \text{ kJ mol}^{-1} \text{ C}^{-1}$) aligns closely with

previous reports ($1.01 \text{ kJ mol}^{-1} \text{ C}^{-1}$ in Hikosaka *et al.*, 2006). A number of potential causes have been suggested for variations in E_{aV} across species, including mesophyll conductance to CO_2 diffusion (Bernacchi *et al.*, 2002; Warren *et al.*, 2007; Walker *et al.*, 2013; von Caemmerer & Evans, 2015), kinetic properties of Rubisco (Yamori *et al.*, 2006), distribution of leaf nitrogen among photosynthetic proteins (Yin *et al.*, 2018) and the influence of other enzymes that affect the *in vivo* activity of Rubisco (Onoda *et al.*, 2005). Furthermore, the Rubisco activation status could also be a significant factor contributing to the observed trends in E_{aV} with T_{growth} , as evidence suggested that plants have the capacity to maintain high Rubisco activation status through an increase in Rubisco activase concentration and expression of heat-stable Rubisco activase isoforms (Crafts-Brandner & Salvucci, 2000; Sage *et al.*, 2008; Yamori *et al.*, 2014). However, not all authors find a change in E_{aV} with growth temperature. Kattge & Knorr (2007) did not find any temperature acclimation in E_{aV} . They argued that the choice of a standard, rather than peaked, Arrhenius model to fit the temperature response for V_{cmax} without considering the deactivation energy would be a possible reason for the observed acclimation responses of E_{aV} in previous studies (e.g. Hikosaka *et al.*, 2006). However, here we used the peaked Arrhenius model, and thus the acclimation of E_{aV} that we observed is not an artifact of model choice.

The second important mechanism for acclimation was a change in the magnitude of JV_{c} , as has also been observed by others (Kattge & Knorr, 2007; Crous *et al.*, 2013, 2018; Lin *et al.*, 2013). The ratio determines the transition between the two limiting steps, W_c and W_j . As the temperature responses of W_c and W_j are different from each other with different optimum temperatures (T_{opt} of $W_c < T_{\text{opt}}$ of W_j), T_{optA} is potentially

determined by the limiting step (von Caemmerer & Farquhar, 1981; Hikosaka, 1997). At higher JV_r , the photosynthetic rate is mostly limited by RuBP carboxylation, and therefore T_{optA} tends to be of a lower value, and vice versa.

The acclimation capacity of ΔS_V observed in this study ($-0.38 \text{ J mol}^{-1} \text{ K}^{-1}$) was lower than the $-1.07 \text{ J mol}^{-1} \text{ K}^{-1} \text{ C}^{-1}$ reported in Kattge & Knorr (2007). The higher sensitivity observed in Kattge & Knorr (2007) could potentially be explained by the lack of variation in E_{aV} . Both E_{aV} and ΔS_V are correlated; a high sensitivity of E_{aV} to T_{growth} could potentially cause ΔS_V to be less sensitive, and vice versa.

We observed changes in JV_r with temperature in all three datasets (Fig. 5), but only the mature plant dataset showed a change in either of the two terms contributing to this ratio. In this dataset, the reduction in JV_r is driven by a reduction in J_{max25} , whereas in the other two datasets, there is no overall effect on either V_{cmax25} or J_{max25} . Some previous studies have observed changes in V_{cmax25} with growth temperature in more limited datasets (Way & Oren, 2010; Lin *et al.*, 2013; Ali *et al.*, 2015; Scafaro *et al.*, 2017; Crous *et al.*, 2018; Smith & Dukes, 2018), but here we did not find any consistent pattern in V_{cmax25} . It appears that JV_r responded strongly and consistently to growth temperature, but whether this is achieved by increasing V_{cmax} , decreasing J_{max} , or both, is highly variable. We speculate that the global pattern in J_{max} observed in Fig. 5(b) may be a response to increasing light availability in the tropics, following the colimitation hypothesis, as proposed by Dong *et al.* (2017), rather than a response to growth temperature.

Improved temperature response functions for photosynthetic capacity

We demonstrate acclimation to growth temperature to be the principal driver, and only a few modest effects of adaptation, in photosynthetic temperature responses at global scale. Our results highlight the limitation of using a fixed set of parameters to determine T_{optA} , and challenge the use of PFT-specific V_{cmax25} and J_{max25} with a fixed set of temperature response parameters without accounting for temperature acclimation and adaptation (Leuning, 2002) in GVMs (Harper *et al.*, 2016; Rogers *et al.*, 2017a). We also demonstrate that the current representation of photosynthetic temperature acclimation (Kattge & Knorr, 2007) that has been implemented in some vegetation models (Smith & Dukes, 2013; Lombardozzi *et al.*, 2015; Smith *et al.*, 2016) was not able to predict the observed patterns in T_{optA} across biomes.

We proposed new algorithms for temperature response that are based on a broad range of data, account for both geographical and temporal variability in photosynthetic biochemical component processes, and are able to capture observed variation of T_{optA} across biomes with a high degree of accuracy. The temperature response functions that we propose have a broad temperature domain (*c.* 3–37°C), which should enable their use in GVMs without outer domain uncertainties (Stinziano *et al.*, 2017), a limitation of the algorithms proposed previously (Kattge & Knorr, 2007) that are widely implemented in GVMs (BETHY,

CLM4.5, Orchidee). As a result of these advantages, our new photosynthetic temperature algorithms provide an improved representation of geographical and temporal variability in T_{optA} and should ultimately improve the accuracy of predicted future C cycle in GVMs.








Acknowledgements







This research was supported by a Western Sydney University PhD scholarship to DPK. AR was supported by the Next Generation Ecosystem Experiments (NGEE Arctic) project, which is supported by the Office of Biological and Environmental Research in the United States Department of Energy (DOE), Office of Science, and through the United States Department of Energy contract no. DE-SC0012704 to Brookhaven National Laboratory. KYC was supported by an Australian Research Council DECRA (DE160101484). DAW acknowledges an NSERC Discovery grant and funding from the Hawkesbury Institute Research Exchange Program. JU, LT and GW were supported by the Swedish strategic research area BECC (Biodiversity and Ecosystem Services in a Changing Climate; www.becc.lu.se). JQC was supported by the NGEE-Tropics, United States DOE. MDK was supported by Australian Research Council Centre of Excellence for Climate Extremes (CE170100023). MS was supported by an Earl S Tupper postdoctoral fellowship. AMJ and JMW were supported by the Biological and Environmental Research Program in the Office of Science, United States DOE under contract DEAC05-00OR22725. MAC was supported by United States DOE grant DE-SC-0011806 and USDA Forest Service 13-JV-11120101-03. Several of the Eucalyptus datasets included in this study were supported by the Australian Commonwealth Department of the Environment or Department of Agriculture, and the Australian Research Council (including DP140103415). We are grateful to Jens Kattge, Yan Shih-Lin, Alida C. Mau and Remko Duursma for useful discussions.

Author contributions

The project was conceived by BEM. The analyses were designed and carried out by DPK with guidance from BEM, JED, MGT, and with contributions from MGDK. Manuscript writing was led by DPK, BEM and JED. All other co-authors (MJA, MB, FJC, KRC, MAC, LAC, JQC, KYC, DND, ED, DSE, OG, QH, KH, AMJ, JW GK, ELK, LMM, YO, PBR, AR, MS, NGS, LT, DTT, HFT, EST, JU, AV, GW, JMW, DAW) contributed data and ideas, and edited the manuscript.

ORCID

Michael J. Aspinwall  <https://orcid.org/0000-0003-0199-2972>
Francisco J. Cano  <https://orcid.org/0000-0001-5720-5865>
Kelsey R. Carter  <https://orcid.org/0000-0001-8327-6413>
Molly A. Cavaleri  <https://orcid.org/0000-0003-0984-611X>
Lucas A. Cernusak  <https://orcid.org/0000-0002-7575-5526>
Jeffrey Q. Chambers  <https://orcid.org/0000-0003-3983-7847>
Kristine Y. Crous  <https://orcid.org/0000-0001-9478-7593>

John E. Drake  <https://orcid.org/0000-0003-1758-2169>
 Erwin Dreyer  <https://orcid.org/0000-0003-4999-5072>
 David S. Ellsworth  <https://orcid.org/0000-0002-9699-2272>
 Oula Ghannoum  <https://orcid.org/0000-0002-1341-0741>
 Anna M. Jensen  <https://orcid.org/0000-0001-5113-5624>
 Martin G. De Kauwe  <https://orcid.org/0000-0002-3399-9098>
 Dushan P. Kumarathunge  <https://orcid.org/0000-0003-1309-4731>
 Belinda E. Medlyn  <https://orcid.org/0000-0001-5728-9827>
 Lina M. Mercado  <https://orcid.org/0000-0003-4069-0838>
 Yusuke Onoda  <https://orcid.org/0000-0001-6245-2342>
 Peter B. Reich  <https://orcid.org/0000-0003-4424-662X>
 Alistair Rogers  <https://orcid.org/0000-0001-9262-7430>
 Martijn Slot  <https://orcid.org/0000-0002-5558-1792>
 Nicholas G. Smith  <https://orcid.org/0000-0001-7048-4387>
 Lasse Tarvainen  <https://orcid.org/0000-0003-3032-9440>
 David T. Tissue  <https://orcid.org/0000-0002-8497-2047>
 Mark G. Tjoelker  <https://orcid.org/0000-0003-4607-5238>
 Danielle A. Way  <https://orcid.org/0000-0003-4801-5319>
 Göran Wallin  <https://orcid.org/0000-0002-5359-1102>

References

- Ali AA, Xu C, Rogers A, McDowell NG, Medlyn BE, Fisher RA, Wullschlegel SD, Reich PB, Vrugt JA, Bauerle WL *et al.* 2015. Global-scale environmental control of plant photosynthetic capacity. *Ecological Applications* 25: 2349–2365.
- Andersson I, Backlund A. 2008. Structure and function of Rubisco. *Plant Physiology and Biochemistry* 46: 275–291.
- Bahar NHA, Hayes L, Scafar AP, Atkin OK, Evans JR. 2018. Mesophyll conductance does not contribute to greater photosynthetic rate per unit nitrogen in temperate compared with tropical evergreen wet-forest tree leaves. *New Phytologist* 218: 492–505.
- Battisti A, Stastny M, Netherer S, Robinet C, Schopf A, Roques A, Larsson S. 2005. Expansion of geographic range in the pine processionary moth caused by increased winter temperatures. *Ecological Applications* 15: 2084–2096.
- Bernacchi CJ, Portis AR, Nakano H, von Caemmerer S, Long SP. 2002. Temperature response of mesophyll conductance. Implications for the determination of Rubisco enzyme kinetics and for limitations to photosynthesis *in vivo*. *Plant Physiology* 130: 1992–1998.
- Bernacchi CJ, Singsaas EL, Pimentel C, Portis AR Jr, Long SP. 2001. Improved temperature response functions for models of Rubisco-limited photosynthesis. *Plant, Cell & Environment* 24: 253–259.
- Berry JA, Björkman O. 1980. Photosynthetic response and adaptation to temperature in higher plants. *Annual Review of Plant Physiology* 31: 491–543.
- Booth BBB, Jones CD, Collins M, Totterdell IJ, Cox PM, Sitch S, Huntingford C, Betts RA, Harris GR, Lloyd J. 2012. High sensitivity of future global warming to land carbon cycle processes. *Environmental Research Letters* 7: 024002.
- von Caemmerer S, Evans JR. 2015. Temperature responses of mesophyll conductance differ greatly between species. *Plant, Cell & Environment* 38: 629–637.
- von Caemmerer S, Farquhar GD. 1981. Some relationships between the biochemistry of photosynthesis and the gas exchange of leaves. *Planta* 153: 376–387.
- Chen MIN, Zhuang Q. 2013. Modelling temperature acclimation effects on the carbon dynamics of forest ecosystems in the conterminous United States. *Tellus B: Chemical and Physical Meteorology* 65: 19156.
- Crafts-Brandner SJ, Salvucci ME. 2000. Rubisco activase constrains the photosynthetic potential of leaves at high temperature and CO₂. *Proceedings of the National Academy of Sciences, USA* 97: 13430–13435.
- Crous KY, Drake JE, Aspinwall MJ, Sharwood RE, Tjoelker MG, Ghannoum O. 2018. Photosynthetic capacity and leaf nitrogen decline along a controlled climate gradient in provenances of two widely distributed *Eucalyptus* species. *Global Change Biology* 24: 4626–4644.
- Crous KY, Quentin AG, Lin YS, Medlyn BE, Williams DG, Barton CV, Ellsworth DS. 2013. Photosynthesis of temperate *Eucalyptus globulus* trees outside their native range has limited adjustment to elevated CO₂ and climate warming. *Global Change Biology* 19: 3790–3807.
- Cunningham SC, Read J. 2002. Comparison of temperate and tropical rainforest tree species: photosynthetic responses to growth temperature. *Oecologia* 133: 112–119.
- De Kauwe MG, Lin Y-S, Wright IJ, Medlyn BE, Crous KY, Ellsworth DS, Maire V, Prentice IC, Atkin OK, Rogers A *et al.* 2016. A test of the 'one-point method' for estimating maximum carboxylation capacity from field-measured, light-saturated photosynthesis. *New Phytologist* 210: 1130–1144.
- Dillaway DN, Kruger EL. 2010. Thermal acclimation of photosynthesis: a comparison of boreal and temperate tree species along a latitudinal transect. *Plant, Cell & Environment* 33: 888–899.
- Dong N, Prentice IC, Evans BJ, Caddy-Retalic S, Lowe AJ, Wright IJ. 2017. Leaf nitrogen from first principles: field evidence for adaptive variation with climate. *Biogeosciences* 14: 481–495.
- Dreyer E, Le Roux X, Montpied P, Daudet FA, Masson F. 2001. Temperature response of leaf photosynthetic capacity in seedlings from seven temperate tree species. *Tree Physiology* 21: 223–232.
- Duursma RA. 2015. Plantecophys – an R package for analysing and modelling leaf gas exchange data. *PLoS ONE* 10: e0143346.
- Falcone DL, Ogas JP, Somerville CR. 2004. Regulation of membrane fatty acid composition by temperature in mutants of Arabidopsis with alterations in membrane lipid composition. *BMC Plant Biology* 4: 17.
- Farquhar GD, von Caemmerer S, Berry JA. 1980. A biochemical model of photosynthetic CO₂ assimilation in leaves of C3 species. *Planta* 149: 78–90.
- Fryer JH, Ledig FT. 1972. Microevolution of the photosynthetic temperature optimum in relation to the elevational complex gradient. *Canadian Journal of Botany* 50: 1231–1235.
- Galmes J, Conesa MA, Diaz-Espejo A, Mir A, Perdomo JA, Niinemets U, Flexas J. 2014. Rubisco catalytic properties optimized for present and future climatic conditions. *Plant Science* 226: 61–70.
- Galmes J, Kapralov MV, Copolovici LO, Hermida-Carrera C, Niinemets Ü. 2015. Temperature responses of the Rubisco maximum carboxylase activity across domains of life: phylogenetic signals, trade-offs, and importance for carbon gain. *Photosynthesis Research* 123: 183–201.
- Gunderson CA, Norby RJ, Wullschlegel SD. 2000. Acclimation of photosynthesis and respiration to simulated climatic warming in northern and southern populations of *Acer saccharum*: laboratory and field evidence. *Tree Physiology* 20: 87–96.
- Gunderson CA, O'Hara KH, Campion CM, Walker AV, Edwards NT. 2009. Thermal plasticity of photosynthesis: the role of acclimation in forest responses to a warming climate. *Global Change Biology* 16: 2272–2286.
- Hall M, Medlyn BE, Abramowitz G, Franklin O, Rantfors M, Linder S, Wallin G. 2013. Which are the most important parameters for modelling carbon assimilation in boreal Norway spruce under elevated [CO₂] and temperature conditions? *Tree Physiology* 33: 1156–1176.
- Harper A, Cox P, Friedlingstein P, Wiltshire A, Jones C, Sitch S, Mercado LM, Groenendijk M, Robertson E, Kattge J *et al.* 2016. Improved representation of plant functional types and physiology in the Joint UK Land Environment Simulator (JULES v4.2) using plant trait information. *Geoscientific Model Development* 2016: 1.
- Hijmans RJ, Cameron SE, Parra JL, Jones PG, Jarvis A. 2005. Very high resolution interpolated climate surfaces for global land areas. *International Journal of Climatology* 25: 1965–1978.
- Hikosaka K. 1997. Modelling optimal temperature acclimation of the photosynthetic apparatus in C-3 plants with respect to nitrogen use. *Annals of Botany* 80: 721–730.
- Hikosaka K, Ishikawa K, Borjigida A, Muller O, Onoda Y. 2006. Temperature acclimation of photosynthesis: mechanisms involved in the changes in temperature dependence of photosynthetic rate. *Journal of Experimental Botany* 57: 291–302.

- Hikosaka K, Murakami A, Hirose T. 1999. Balancing carboxylation and regeneration of ribulose-1,5-bisphosphate in leaf photosynthesis: temperature acclimation of an evergreen tree, *Quercus myrsinaefolia*. *Plant, Cell & Environment* 22: 841–849.
- Huner NPA. 1985. Morphological, anatomical, and molecular consequences of growth and development at low temperature in *Secale cereale* L. cv. Puma. *American Journal of Botany* 72: 1290–1306.
- Huner NPA, Macdowall FDH. 1979. Changes in the net charge and subunit properties of ribulose bisphosphate carboxylase–oxygenase during cold hardening of Puma rye. *Canadian Journal of Biochemistry* 57: 155–164.
- Johnson FH, Eyring H, Williams RW. 1942. The nature of enzyme inhibitions in bacterial luminescence: sulfanilamide, urethane, temperature and pressure. *Journal of Cellular and Comparative Physiology* 20: 247–268.
- Kattge J, Knorr W. 2007. Temperature acclimation in a biochemical model of photosynthesis: a reanalysis of data from 36 species. *Plant, Cell & Environment* 30: 1176–1190.
- Kumarathunge DP, Medlyn BE, Drake JE, Tjoelker MG, Aspinwall MJ, Battaglia M, Cano FJ, Carter KR, Molly AC, Lucas AC *et al.* 2018. ACI-TGlob_V1.0: A Global dataset of photosynthetic CO₂ response curves of terrestrial plants. doi: 10.6084/m9.figshare.7283567.v1
- Lambers H, Chapin FS, Pons TL. 2008. *Plant physiological ecology*. New York, NY, USA: Springer.
- Ledig FT, Korbobo DR. 1983. Adaptation of sugar maple populations along altitudinal gradients: photosynthesis, respiration, and specific leaf weight. *American Journal of Botany* 70: 256–265.
- Leuning R. 2002. Temperature dependence of two parameters in a photosynthesis model. *Plant, Cell & Environment* 25: 1205–1210.
- Lin Y-S, Medlyn BE, De Kauwe MG, Ellsworth DS. 2013. Biochemical photosynthetic responses to temperature: how do interspecific differences compare with seasonal shifts? *Tree Physiology* 33: 793–806.
- Lin Y-S, Medlyn BE, Duursma RA, Prentice IC, Wang H, Baig S, Eamus D, de Dios Victor R, Mitchell P, Ellsworth DS *et al.* 2015. Optimal stomatal behaviour around the world. *Nature Climate Change* 5: 459.
- Lin Y-S, Medlyn BE, Ellsworth DS. 2012. Temperature responses of leaf net photosynthesis: the role of component processes. *Tree Physiology* 32: 219–231.
- Lombardozzi DL, Bonan GB, Smith NG, Dukes JS, Fisher RA. 2015. Temperature acclimation of photosynthesis and respiration: a key uncertainty in the carbon cycle-climate feedback. *Geophysical Research Letters* 42: 8624–8631.
- Medlyn BE, Dreyer E, Ellsworth D, Forstreuter M, Harley PC, Kirschbaum MUF, Le Roux X, Montpied P, Strassmeyer J, Walcroft A *et al.* 2002a. Temperature response of parameters of a biochemically based model of photosynthesis. II. A review of experimental data. *Plant, Cell & Environment* 25: 1167–1179.
- Medlyn BE, Loustau D, Delzon S. 2002b. Temperature response of parameters of a biochemically based model of photosynthesis. I. Seasonal changes in mature maritime pine (*Pinus pinaster* Ait.). *Plant, Cell & Environment* 25: 1155–1165.
- Medlyn BE, Pepper DA, O'Grady AP, Keith H. 2007. Linking leaf and tree water use with an individual-tree model. *Tree Physiology* 27: 1687–1699.
- Mercado LM, Medlyn BE, Huntingford C, Oliver RJ, Clark DB, Stephen S, Przemyslaw Z, Kattge J, Harper AB, Cox PM. 2018. Large sensitivity in land carbon storage due to geographical and temporal variation in the thermal response of photosynthetic capacity. *New Phytologist* 218: 1462–1477.
- Nakagawa S, Schielzeth H. 2013. A general and simple method for obtaining R² from generalized linear mixed-effects models. *Methods in Ecology and Evolution* 4: 133–142.
- Onoda Y, Hikosaka K, Hirose T. 2005. The balance between RuBP carboxylation and RuBP regeneration: a mechanism underlying the interspecific variation in acclimation of photosynthesis to seasonal change in temperature. *Functional Plant Biology* 32: 903–910.
- R Development Core Team. 2012. *R: a language and environment for statistical computing*. Vienna, Austria: R Foundation for Statistical Computing.
- Rehfeldt GE, Wykoff WR, Ying CC. 2001. Physiologic plasticity, evolution, and impacts of a changing climate on *Pinus contorta*. *Climatic Change* 50: 355–376.
- Reich PB, Sendall KM, Rice K, Rich RL, Stefanski A, Hobbie SE, Montgomery RA. 2015. Geographic range predicts photosynthetic and growth response to warming in co-occurring tree species. *Nature Climate Change* 5: 148.
- Robakowski P, Li Y, Reich PB. 2012. Local ecotypic and species range-related adaptation influence photosynthetic temperature optima in deciduous broadleaved trees. *Plant Ecology* 213: 113–125.
- Rogers A, Humphries SW. 2000. A mechanistic evaluation of photosynthetic acclimation at elevated CO₂. *Global Change Biology* 6: 1005–1011.
- Rogers A, Medlyn BE, Dukes JS, Bonan G, von Caemmerer S, Dietze MC, Kattge J, Leakey ADB, Mercado LM, Niinemets Ü *et al.* 2017a. A roadmap for improving the representation of photosynthesis in Earth system models. *New Phytologist* 213: 22–42.
- Rogers A, Serbin SP, Ely KS, Sloan VL, Wullschlegel SD. 2017b. Terrestrial biosphere models underestimate photosynthetic capacity and CO₂ assimilation in the Arctic. *New Phytologist* 216: 1090–1103.
- Sage RF, Way DA, Kubien DS. 2008. Rubisco, Rubisco activase, and global climate change. *Journal of Experimental Botany* 59: 1581–1595.
- Savir Y, Noor E, Milo R, Tlustý T. 2010. Cross-species analysis traces adaptation of Rubisco toward optimality in a low-dimensional landscape. *Proceedings of the National Academy of Sciences, USA* 107: 3475–3480.
- Scafaro AP, Xiang S, Long BM, Bahar NHA, Weerasinghe LK, Creek D, Evans JR, Reich PB, Atkin OK. 2017. Strong thermal acclimation of photosynthesis in tropical and temperate wet-forest tree species: the importance of altered Rubisco content. *Global Change Biology* 23: 2783–2800.
- Sendall KM, Reich PB, Zhao C, Jihua H, Wei X, Stefanski A, Rice K, Rich RL, Montgomery RA. 2015. Acclimation of photosynthetic temperature optima of temperate and boreal tree species in response to experimental forest warming. *Global Change Biology* 21: 1342–1357.
- Sharkey TD, Bernacchi CJ, Farquhar GD, Singsaas EL. 2007. Fitting photosynthetic carbon dioxide response curves for C-3 leaves. *Plant, Cell & Environment* 30: 1035–1040.
- Slatyer R. 1977. Altitudinal variation in the photosynthetic characteristics of snow gum, *Eucalyptus pauciflora* Sieb. Ex Spreng. III. Temperature response of material grown in contrasting thermal environments. *Functional Plant Biology* 4: 301–312.
- Slatyer R. 1978. Altitudinal variation in the photosynthetic characteristics of snow gum, *Eucalyptus pauciflora* Sieb. Ex Spreng. VII. Relationship between gradients of field temperature and photosynthetic temperature optima in the snowy mountains area. *Australian Journal of Botany* 26: 111–121.
- Slot M, Winter K. 2017. *In situ* temperature relationships of biochemical and stomatal controls of photosynthesis in four lowland tropical tree species. *Plant, Cell & Environment* 40: 3055–3068.
- Smith NG, Dukes JS. 2013. Plant respiration and photosynthesis in global-scale models: incorporating acclimation to temperature and CO₂. *Global Change Biology* 19: 45–63.
- Smith NG, Dukes JS. 2017. Short-term acclimation to warmer temperatures accelerates leaf carbon exchange processes across plant types. *Global Change Biology* 23: 4840–4853.
- Smith NG, Dukes JS. 2018. Drivers of leaf carbon exchange capacity across biomes at the continental scale. *Ecology* 99: 1610–1620.
- Smith NG, Lombardozzi D, Tawfik A, Bonan G, Dukes JS. 2017. Biophysical advances of photosynthetic temperature acclimation for climate. *Journal of Advances in Modeling Earth Systems* 9: 536–547.
- Smith NG, Malyshev SL, Shevliakova E, Kattge J, Dukes JS. 2016. Foliar temperature acclimation reduces simulated carbon sensitivity to climate. *Nature Climate Change* 6: 407–411.
- Stinziano JR, Way DA, Bauerle WL. 2017. Improving models of photosynthetic thermal acclimation: which parameters are most important and how many should be modified? *Global Change Biology* 24: 1580–1598.
- Tan ZH, Jiye Z, Yong-Jiang Z, Martijn S, Minoru G, Takashi H, Yoshiko K, Humberto RdR, Scott RS, Michael LG *et al.* 2017. Optimum air temperature for tropical forest photosynthesis: mechanisms involved and implications for climate warming. *Environmental Research Letters* 12: 054022.
- Tcherkez GGB, Farquhar GD, Andrews TJ. 2006. Despite slow catalysis and confused substrate specificity, all ribulose biphosphate carboxylases may be nearly perfectly optimized. *Proceedings of the National Academy of Sciences, USA* 103: 7246–7251.
- Valladares F, Matesanz S, Guilhaumon F, Araújo MB, Balaguer L, Benito-Garzon M, Cornwell W, Gianoli E, van Kleunen M, Naya DE *et al.* 2014. The effects of phenotypic plasticity and local adaptation on

- forecasts of species range shifts under climate change. *Ecology Letters* 17: 1351–1364.
- Värhammar A, Wallin G, McLean CM, Dusenge ME, Medlyn BE, Hasper TB, Nsabimana D, Uddling J. 2015. Photosynthetic temperature responses of tree species in Rwanda: evidence of pronounced negative effects of high temperature in montane rainforest climax species. *New Phytologist* 206: 1000–1012.
- Walker B, Ariza LS, Kaines S, Badger MR, Cousins AB. 2013. Temperature response of *in vivo* Rubisco kinetics and mesophyll conductance in *Arabidopsis thaliana*: comparisons to *Nicotiana tabacum*. *Plant, Cell & Environment* 36: 2108–2119.
- Warren CR, Löw M, Matyssek R, Tausz M. 2007. Internal conductance to CO₂ transfer of adult *Fagus sylvatica*: variation between sun and shade leaves and due to free-air ozone fumigation. *Environmental and Experimental Botany* 59: 130–138.
- Way DA, Oren R. 2010. Differential responses to changes in growth temperature between trees from different functional groups and biomes: a review and synthesis of data. *Tree Physiology* 30: 669–688.
- Way DA, Sage RF. 2008. Thermal acclimation of photosynthesis in black spruce [*Picea mariana* (Mill.) B.S.P.]. *Plant, Cell & Environment* 31: 1250–1262.
- Way DA, Stinziano JR, Berghoff H, Oren R. 2017. How well do growing season dynamics of photosynthetic capacity correlate with leaf biochemistry and climate fluctuations? *Tree Physiology* 37: 879–888.
- Way DA, Yamori W. 2014. Thermal acclimation of photosynthesis: on the importance of adjusting our definitions and accounting for thermal acclimation of respiration. *Photosynthesis Research* 119: 89–100.
- Yamaguchi DP, Nakaji T, Hiura T, Hikosaka K. 2016. Effects of seasonal change and experimental warming on the temperature dependence of photosynthesis in the canopy leaves of *Quercus serrata*. *Tree Physiology* 36: 1283–1295.
- Yamori W, Hikosaka K, Way DA. 2014. Temperature response of photosynthesis in C₃, C₄, and CAM plants: temperature acclimation and temperature adaptation. *Photosynthesis Research* 119: 101–117.
- Yamori W, Noguchi K, Terashima I. 2005. Temperature acclimation of photosynthesis in spinach leaves: analyses of photosynthetic components and temperature dependencies of photosynthetic partial reactions. *Plant, Cell & Environment* 28: 536–547.
- Yamori W, Sakata N, Suzuki Y, Shikanai T, Makino A. 2011. Cyclic electron flow around photosystem I via chloroplast NAD(P)H dehydrogenase (NDH) complex performs a significant physiological role during photosynthesis and plant growth at low temperature in rice. *The Plant Journal* 68: 966–976.
- Yamori W, Suzuki K, Noguchi KO, Nakai M, Terashima I. 2006. Effects of Rubisco kinetics and Rubisco activation state on the temperature dependence of the photosynthetic rate in spinach leaves from contrasting growth temperatures. *Plant, Cell & Environment* 29: 1659–1670.
- Yin X, Schapendonk AHCM, Struik PC. 2018. Exploring the optimum nitrogen partitioning to predict the acclimation of C₃ leaf photosynthesis to varying growth conditions. *Journal of Experimental Botany*. doi: 10.1093/jxb/ery277
- Zuur AF, Ieno EN, Walker NJ, Saveliev A, Smith GM. 2009. *Mixed effects models and extensions in ecology with R*. New York, NY, USA: Springer Science & Business Media.

Supporting Information

Additional Supporting Information may be found online in the Supporting Information section at the end of the article:

Fig. S1 Distribution of the dataset used in this study.

Fig. S2 Relationship between apparent V_{cmax} and J_{max} values derived using two AC_i curve-fitting routines, with and without accounting for TPU limitation.

Fig. S3 Temperature response parameters of photosynthetic respiratory component processes.

Fig. S4 $R_{\text{L25}} : V_{\text{cmax25}}$ ratio at a standard leaf temperature of 25°C.

Table S1 List of data sources.

Table S2 Results of the linear mixed-effects models fitted for the common-garden dataset to test for adaptation of photosynthetic temperature response parameters to species' climate of origin.

Table S3 Results of the linear regression analysis between observed and modelled temperature optimum for photosynthesis at a fixed C_i of 275 $\mu\text{mol mol}^{-1}$ using model parameterizations given in Table 2 in the main text and the Kattge & Knorr (2007) algorithm.

Please note: Wiley Blackwell are not responsible for the content or functionality of any Supporting Information supplied by the authors. Any queries (other than missing material) should be directed to the *New Phytologist* Central Office.